Evaluation of Different Additives in a Polyolefin System and Their Impact on the Polymer Properties

Master's thesis in Materials Chemistry

Sara Razdan

DEPARTMENT OF CHEMISTRY AND CHEMICAL ENGINEERING
CHALMERS UNIVERSITY OF TECHNOLOGY
Gothenburg, Sweden 2025
www.chalmers.se

Master's thesis 2025

Evaluation of Different Additives in a Polyolefin System and Their Impact on the Polymer Properties

SARA RAZDAN

CHALMERS
UNIVERSITY OF TECHNOLOGY

Borealis AB Innovation Center
Department of Chemistry and Chemical Engineering
Chalmers University of Technology
Gothenburg, Sweden 2025

Evaluation of Different Additives in a Polyolefin System and Their Impact on the Polymer Properties
SARA RAZDAN

Supervisors: Tina Gschneidtner, Borealis AB.
Przemyslaw Sowinski, Department of Chemistry and Chemical Engineering
Examiner: Christian Müller, Department of Chemistry and Chemical Engineering

Master's Thesis 2025
Borealis AB.
Innovation Center
Department of Chemistry and Chemical Engineering
Chalmers University of Technology
SE-412 96 Gothenburg
Telephone +46 31 772 1000

Gothenburg, Sweden 2025

Evaluation of Different Additives in a Polyolefin System and Their Impact on the Polymer Properties

Sara Razdan
Department of Chemistry and Chemical Engineering
Chalmers University of Technology

Abstract

The effect of various liquid and solid additives on the physical properties of a heterophasic PP copolymer were studied. Two sample preparation methods, compression molding and tape extrusion were used to study the mechanical and thermal properties of the polymer. To investigate the material properties, Wide Angle X-ray Scattering (WAXS), Small Angle X-ray Scattering (SAXS), Dynamic Mechanical Thermal Analysis (DMTA), Tensile test, Transient Plane Source (TPS) were performed. The incorporation of additives in polymer samples did not exhibit a considerable influence on the thermal properties of blends; however it affected the mechanical properties. The presence of liquid additives in the interlamellar distance may result in an increase in the interlamellar distance without a notable impact on lamellar thickness, as laterally investigated and confirmed by SAXS results. The liquid in amorphous phase decreases the modulus of the sample. Increasing interlamellar distance influenced the plastic deformation mechanism by decreasing yield stress. The additives exhibited a plasticizing effect on the polymer, reducing modulus in the testing temperature range, leading to an improvement in mechanical properties without compromising the thermal stability of the polymer blend. The additives did not affect the degree of crystallinity, despite the changes in kinetics of crystallization. The introduction of additives to the polymer did not cause a significant change in the degree of crystallinity; however, a higher cooling rate in the Tape extrusion sample preparation method led to crystallographic variations and a reduction in the content of γ- form.

Keywords: Polyolefin, Additive, mechanical properties, thermal conductivity

Acknowledgements

I gratefully acknowledge everyone who contributed to this master's thesis project, namely:
Przemyslaw Sowinski, my academic supervisor at Chalmers, for his insightful guidance, provision of valuable ideas, and for his deep knowledge and experience that supported me throughout this project.
Tina Gschneidtner, my industrial supervisor at Borealis, for her unfailing support, valuable contributions throughout this project, and for facilitating progress of the work at the company.
I would like to thank Per-Ola Hagstrand and his professional research team for offering this opportunity, as well as Borealis stenungsund, for creating a safe, warm, and welcoming working environment through my learning journey in this project. Special thanks to amazing people in the mechanical lab led by Jennie Antonsson, to Johan Andersson for his expertise, and to Nils Carlsson main in the analytical lab for his valuable guidance. A heartfelt thanks to Alex Porota for his valuable assistance.
Many thanks to professor Müller and his research group for their invaluable feedback and for generously sharing their expertise throughout this project.
Last but not least, I would like to thank my supportive parents Jila and Hassan, without their patience and unconditional love, I would not have come this far.

Sara Razdan, Gothenburg, June 2025

Abbreviations

Below is the list of abbreviations that have been used throughout this thesis:

HDPE	High-density polyethylene
LDPE	Low-density polyethylene
iPP	Isotactic polypropylene
PP	Polypropylene
PE	Polyethylene
NP	Heterophasic PP copolymer
sPP	Syndiotactic polypropylene
MC	Metallocene catalyst
ZN	Ziegler-Natta catalyst
MWD	Molecular weight distribution
MW	Molecular weight
ATR	Attenuated total reflection
TE	Tape Extrusion
CM	Compression Molding
LA.A	Liquid Additive A
LA.B	Liquid Additive B
LA.C	Liquid Additive C
LA.D	Liquid Additive D
LA.E	Liquid Additive E
LA.F	Liquid Additive F
LA.H	Liquid Additive H
SA.I	Solid Additive I
SA.K	Solid Additive K
LA.M	Liquid Additive M
LA.N	Liquid Additive N
SA.P	Solid Additive P
P.A	Polymer blended with liquid additive A
P.B	Polymer blended with liquid additive B
P.C	Polymer blended with liquid additive C
P.D	Polymer blended with liquid additive D
P.E	Polymer blended with liquid additive E
P.F	Polymer blended with liquid additive F
P.H	Polymer blended with liquid additive H
P.I	Polymer blended with solid additive I
P.K	Polymer blended with solid additive K
P.M	Polymer blended with liquid additive M
P.N	Polymer blended with liquid additive N
P.P	Polymer blended with solid additive P

Nomenclature

Below is the nomenclature of indices, sets, parameters, and variables that have been used throughout this thesis.

Parameters

C_v	Specific heat capacity at constant volume
u	Speed of phonon
L	Mean free path of phonon
α	Thermal diffusivity
λ	Wavelength
n_1, n_2	Refractive indices
c	Concentration
C	Heat capacity
m	Mass
κ	Sensitivity of thermal measurement
t	Duration of the test
p_o	Power output of sensor
r	Radius of the largest wire ring
A_0	Initial cross-section area
E	Young's modulus
l_p	Long period
ΔH_m^0	Melting enthalpy of fully crystalline polymer
d	Sample thickness
a	Cross-section area

Variables

K	Thermal conductivity
ρ	Density
T	Temperature
ΔT	Temperature change
d_p	Penetration depth
θ	Angle of incidence
A	Absorbance
ε	extinction coefficient, strain
q	Scattering vector
E'	Storage modulus
E"	Loss modulus
E_0	Strain at yield
δ	Phase difference between stress and strain
ι	Optical path length
ΔQ	Change in heat energy
ΔT	Temperature difference
λ	Duration of the test
σ	Stress
F	Force
ΔH_m	Melting enthalpy of the sample
X	Degree of crystallinity

Contents

List of Acronyms **ix**

Nomenclature **xii**

List of Figures **xvi**

List of Tables **xix**

1 Introduction **1**
1.1 Aim of study . . . 1

2 Background **2**
2.1 Polymer properties . . . 2
2.1.1 Polyolefin . . . 2
2.1.2 Polymerization . . . 4
2.1.3 Crystallization . . . 5
2.1.4 Thermal conductivity . . . 7
2.1.5 Mechanical properties . . . 8
2.2 Additives . . . 8
2.2.1 Liquid Additive A . . . 8
2.2.2 Liquid Additive B . . . 9
2.2.3 Liquid Additive C . . . 9
2.2.4 Liquid Additive D . . . 9
2.2.5 Liquid Additive E . . . 9
2.2.6 Liquid Additive F . . . 9
2.2.7 Liquid Additive H . . . 9
2.2.8 Solid Additive I . . . 9
2.2.9 Solid Additive K . . . 9
2.2.10 Liquid Additive M . . . 10
2.2.11 Liquid Additive N . . . 10
2.2.12 Solid Additive P . . . 10
2.3 Analyzing methods . . . 10
2.3.1 Thermogravimetric Analysis (TGA) . . . 10
2.3.2 Fourier Transform Infrared Spectroscopy (FTIR) . . . 10
2.3.3 Differential Scanning Calorimetry (DSC) . . . 11
2.3.4 Transient Plane Source (TPS) . . . 12
2.3.5 X-Ray Scattering . . . 13

2.3.6 Mechanical Testing . . . 13
2.3.7 Dynamic Mechanical Thermal Analysis . . . 14

3 Methods **16**
3.1 Compounding . . . 16
3.1.1 Addition . . . 17
3.2 Thermogravimetry . . . 18
3.3 Saturation Concentration/ Exudation Test . . . 18
3.4 Fourier Transform Infrared Spectroscopy . . . 18
3.5 Sample Preparation . . . 19
3.5.1 Tape Extrusion . . . 19
3.5.2 Compression Molding . . . 19
3.6 Differential Scanning Calorimetry . . . 20
3.7 Transient Plane Source . . . 20
3.8 Small Angle X-Ray Scattering . . . 21
3.9 Wide Angle X-Ray Scattering . . . 21
3.10 Mechanical Testing . . . 22
3.11 Dynamic Mechanical Thermal Analysis . . . 22

4 Results and Discussion **23**
4.1 Material Examination . . . 23
4.1.1 Thermal Stability . . . 23
4.1.1.1 Thermal Stability of the LAs and SAs . . . 23
4.1.1.2 Thermal Stability of the Polymer Blends . . . 25
4.1.2 Saturation Concentration Test . . . 26
4.1.3 Fourier Transform Infrared Spectroscopy . . . 29
4.1.4 Kinetics of Crystallization . . . 31
4.1.5 DSC of Compression Molded and Tape Extruded Samples . . . 34
4.1.6 Wide Angle X-Ray Scattering . . . 36
4.1.7 Small Angle X-Ray Scattering . . . 38
4.2 Material Properties . . . 41
4.2.1 Thermal Conductivity by Transient Plane Source . . . 41
4.2.2 Dynamic Mechanical Thermal Analysis . . . 43
4.2.3 Mechanical Testing . . . 47

5 Conclusion **52**

Bibliography **53**

List of Figures

2.1 Tacticity in PP, arranged from top to bottom: the structure of isotactic, syndiotactic and atactic polypropylene 3
2.2 Schematic representation of a spherulite. 3
2.3 Example of internal electron donor, Phthalte. 4
2.4 Schematic representation of three regimes of crystallization. 5
2.5 Sample fixed between clamps of DMA 15

3.1 P.M3% after 6 hours impregnation 17
3.2 NP without LA, NP specimens submerged in LA.H, LA.F, LA.M and LA.C. 18
3.3 The Dumbbell-shape specimen (5A specimen) for tensile test. 22

4.1 5% decrease in the weight of LAs and SAs. 23
4.2 Weight% of LAs and SAs vs. Temperature. SA.K (dark brown curve), LA.D (orange curve), and LA.G (light green curve). 24
4.3 Weight loss% of NP and polymer blends at 400°C. 25
4.4 Weight% of the polymer blends vs. temperature. NP (green curve), P.K3% (dark brown curve), P.I3% (pink curve), and P.A6% (red curve). 25
4.5 Weight increase vs. Time 26
4.6 Melting temperature T_m and crystalline mass fraction X of NP after 340 hours of submersion in various LAs. 27
4.7 Crystallization temperatures T_c1 and T_c2 of NP after 340 hours of submersion in various LAs. 27
4.8 Melting point depression vs. LA content in NP. No LA (green pint), LA.D (orange point), LA.M (burgundy point), LA.B (light brown point), and LA.A (red point). 28
4.9 Comparison of absorbance spectra of NP (green) with P.I3% (red), subtraction of both spectras (blue) and spectra of SA.I (black). . . . 29
4.10 Comparison of absorbance spectra of NP (green) with P.E1% (red), subtraction (blue) and LA.E (black). 29
4.11 Heat flow curves as a function of time for P.K3%(brown curve), P.P3% (violet curve) and P.A3% (light red curve), NP(green curve). Isothermal crystallization at 130°C. 31
4.12 Additive content vs. Half time of crystallization. NP(green), P.A1% (light orange), P.A3% (light red), and P.A6% (red). 32

4.13 Plots of ln(-ln(1/1- α) vs. ln(t) for NP (green curve), P.A1% (light orange curve), P.A3% (light red curve), and P.A6% (red curve). The curves are vertically shifted for clarity and better illustration. 33
4.14 Melting temperature T_m and crystalline mass fraction X of NP and melt-blended samples, determined by DSC. Compression molding samples. 34
4.15 Melting temperature T_m and crystalline mass fraction X of NP and melt-blended samples, determined by DSC. Tape extrusion samples. . 35
4.16 Comparison of first heating curve of NP (green curve) with P.I1% (pink curve), determined by DSC. Compression molding samples. . . 35
4.17 Comparison of first heating curve of NP (green curve) with P.I1% (pink curve), determined by DSC. Tape extrusion samples. 36
4.18 Wide angle X-ray scattering diffractogram. NP prepared by CM (green curve), P.A6% prepared by CM (red curve), P.A6% prepared by TE (red dotted curve). 36
4.19 Scattering profile of P.A6% and P.E3% in comparison with NP. P.A6% (red), P.E3% (blue) and NP (green). 38
4.20 Long period and lamellar thickness of the NP and blends, determined by DSC. Compression molding samples. 39
4.21 Crystalline mass fraction and density of the NP and blends, determined by DSC. Compression molding samples. 39
4.22 Long period variations with additive content. P.A (red), P.E (blue) and NP (green). 40
4.23 Thermal Conductivity of LAs and SAs in comparison with NP tested at 23±0,3°C. 41
4.24 Thermal Conductivity of polymer blends in comparison with NP tested at 23±0,3°C. 42
4.25 DMA storage modulus for polymer blends and NP at -40°C. 43
4.26 DMA storage modulus for polymer blends and NP at 25°C. 44
4.27 DMA storage modulus for polymer blends and NP at 130°C. 44
4.28 Glass transition temperature T_g of the polymer matrix and the rubber phase in NP and other polymer blends. 45
4.29 Comparison of glass transition temperatures for NP (green) and P.A6% (red). 46
4.30 Comparison of variations in glass transition temperature of matrix and rubber phase. Rubber phase in black color and matrix in red color. 46
4.31 Stress-Strain curve recorded during tensile deformation. NP (green curve), P.I3% (pink curve), P.P3% (violet curve), P.E3% (blue curve), P.A6% (red curve). 47
4.32 Mechanical properties of different tape extruded polymer blends . . . 48
4.33 Mechanical properties of different tape extruded polymer blends . . . 48
4.34 Stress-Strain curve recorded during tensile deformation. NP (green curve), P.I3% (pink curve), P.P3% (violet curve), P.E3% (blue curve), P.A6% (red curve). 49
4.35 Comparison of tensile modulus with varying content for LA.E (blue), LA.A (red), SA.I (pink) and SA.P (violet) in blend with NP(green). . 49

4.36 Comparison of yield stress with varying content for LA.E (blue), LA.A (red), SA.I (pink) and SA.P (violet) in blend with NP (green). 50
4.37 Yield stress vs. long period. NP (green), P.P3% (violet), P.I3% (pink), P.E3% (blue), and P.A6% (red). 50

List of Tables

3.1 List of Polymer blends 17

4.1 The additive content assessed using IR-spectra in ATR mode. 30
4.2 The additive content assessed using IR-spectra in transmission mode using Beer-Lambert law. 30
4.3 Isothermal crystallization parameters of NP, P.A1%, P.A3%, and P.A6%. Standard error for the linear fitting is reported. 32

1
Introduction

There are several approaches to modify PP; one of them is the introduction of additives into the polymer matrix. Additives are basically used to modify base polymers, achieving desirable properties and performance. Different processing conditions are required depending on their properties, such as thermal stability or their interaction with the polymer. With the optimal content and uniform incorporation of a suitable additive into the polymer matrix, consistent properties can be achieved throughout the material [1].
The additives can be classified based on their application. They can enhance the thermal stability of polymers in the processing stage. Some provide added value and offer performance benefits that outweigh their cost. Others may improve both the processing and mechanical properties. In this context, special additives are designed to complement and balance the effects of the other additives, addressing their weaknesses to ensure better overall functionality and enhance the stability of the material [2].

1.1 Aim of study

This project aimed to understand the effects of different additives on a selection of physical properties of a polymer. To achieve this, the additives were incorporated into the polymer matrix, and the resulting mixtures were evaluated for their thermal and mechanical properties.
In order to understand the role of the additives, the thermal properties of the samples were investigated using the transient plane source method, and their mechanical properties were evaluated through tensile testing and dynamic mechanical thermal analysis. The additive content was quantified through Fourier Transform Infrared Spectroscopy test.

2
Background

2.1 Polymer properties

2.1.1 Polyolefin

PP and PE based polymers belong to the polyolefin class of polymers. Due to their versatile properties, including recyclability and low price, they have a high share of the market. However, some shortcomings of PP, such as its brittleness, rigidity and poor low-temperature impact resistance, limit its use in certain applications. There are several approaches to improve the material properties, such as copolymerization or blending with other polyolefins or other polymers [3]. The presence of amorphous and crystalline regions in PP and PE polymers results in the formation of a semicrystalline structure. In the crystalline region, the chains are highly arranged relative to each other, forming an ordered structure. Strong covalent bonds along the chain and Van der Waals forces between chains hold them together. In contrast, entangled random chains can move more freely in the amorphous region. The chemical structure of the polymer chain and structural irregularities influence its crystallization [4]. Entanglements or bulky side groups can limit the free movement of chains, and they may not be able to arrange themselves in an ordered structure and remain in the amorphous region. For example, high-density polyethylene (HDPE) with few short branches compared to low-density polyethylene (LDPE) with long side branches and with a higher content of short chain branches, exhibits a higher degree of crystallinity. This is basically influenced by the structure of HDPE, which allows the chains to organize themselves into a more compact structure. This results in a denser material with a higher degree of crystallinity. How the material crystallizes determine the physical,and mechanical properties.

For propylene- based polyolefins, the choice of catalyst plays a critical role in controlling the spatial arrangement (tacticity) of the polymer chain. This controls the formation of isotactic (iPP), syndiotactic (sPP), or atactic (aPP) polypropylene, which differ in the arrangement of the side group. Tacticity affects crystallization and, consequently, the properties of the material [4]. A low crystallinity in aPP results in a waxy texture that is characterized by poor mechanical stability and low thermal conductivity, while the iPP is known for its stiffness and superior mechanical and thermal properties. SPP crystallizes with a low degree of crystallinity. Therefore, it possesses intermediate mechanical properties between aPP and iPP. As shown in Fig. 2.1, the arrangement of the methyl side groups in iPP creates an ordered structure and results in a higher

crystallinity (better packing) compared to aPP with a less regular structure [3].

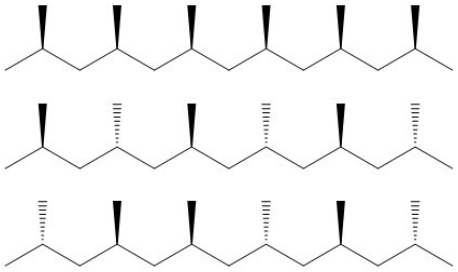

Figure 2.1: Tacticity in PP, arranged from top to bottom: the structure of isotactic, syndiotactic and atactic polypropylene

Single crystals in lamellar shape can form from a melt or polymer solution. The lamellar thickness and crystallographic structure define the melting temperature of the material, and the variations in its distribution can result in a wide range of melting peaks. The processing conditions, such as temperature and cooling rate, basically determine the lamellar thickness. Crystallization at higher temperatures or through a slow cooling process can lead to an increase in lamellar thickness, resulting in a higher melting temperature [5]. Additionally, introducing side chains (branches) or comonomers into the polymer chain affects the crystal structure, can reduce the lamellar thickness, and consequently lowers the melting temperature [6][3].

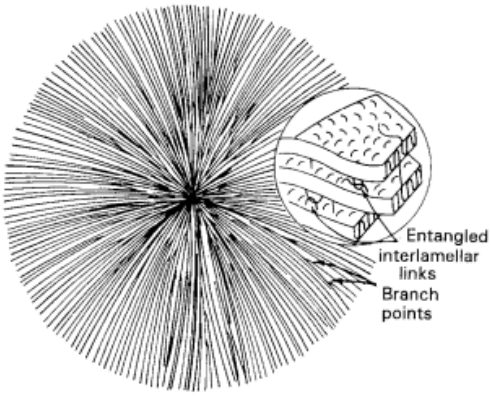

Figure 2.2: Schematic representation of a spherulite; the crystalline lamellae originating from nucleus in all directions. Reproduced with permission: 1994, Springer Verlag [5].

Impurities, disordered tacticity, monomer, catalyst residues, and density fluctuations can act as nuclei and initiate crystal growth. As presented in Fig. 2.2, spherulites are crystalline aggregates that form during the crystallization process and consist of crystalline lamellae growing in all directions. Lamellae are separated by amorphous regions. The size of the spherulites and, therefore, nucleation density influences the microscopic properties of the polymer, such as clarity or barrier properties.

2.1.2 Polymerization

Isotactic polypropylene is a widely used polymer. It has a remarkable resistance to moisture and chemicals with superior mechanical and thermal properties. Its advantages also include good processability and low production cost.
Discovery of the Ziegler-Natta catalyst (ZN) enabled the polymerization of iPP, and the introduction of the homogeneous metallocene catalyst (MC) offered improvements in terms of better control over molecular weight distribution and the sequence of repeating units in the macromolecules [4]. Homopolymerization of propene or copolymerization with another monomer in the presence of chromium, ZN or MC catalyst is an approach to modify the thermal and mechanical properties of PP. Heterophasic PP copolymer consists of ethylene-propylene copolymer with a low ethylene content, and a dispersed phase consisting of ethylene-propylene copolymer(EPC) with a high concentration of ethylene comonomer. The dispersed phase is also commonly called ethylene- propylene rubber (EPR) due to the mechanical properties similar to elastomers. The compatibility between matrix and dispersed phase depends on the amount of the comonomer in both phases. This can be improved by both chemical composition and molecular weight (MW) of the phases [7][8]. Heterophasic PP copolymer polymerization using ZN catalyst, in a multiple-reactor system called Borstar or Spheripol PP process provides an economical method for designing polymers with precise shape, controlled morphology and optimized properties. In this method, processing conditions are independently adjustable for each reactor. The process normally starts with pre-polymerization in the presence of the catalyst suspension. This step is designed to achieve a better distribution of the catalyst particles, and the polymerization occurs on the surface of the particles. The polymer will be transferred to the loop reactor. The Continuous phase, consisting of ethylene-propylene random-copolymer (liquid phase), will be directed to multiple gas-phase reactors to complete the polymerization through the inclusion of the rubber phase. The incorporation and design of spherical dispersed rubber phases, differing in size or composition, occurs in multiple reactors, can result in products with different morphology and balanced mechanical properties [9][10]. The mechanism of polymerization and catalyst structure, including a combination of internal and external electron donors, together with the catalyst activator, which also removes impurities, determine the microstructure of the polymer. Internal electron donors together with external electron donors ensure the precise stereoregularity of the polymer, provide higher yield and better control over molecular weight distribution (MWD) [8][10]. An example of internal electron donors is presented in Fig. 2.3.

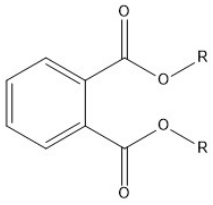

Figure 2.3: Example of internal electron donor, Phthalte.

2.1.3 Crystallization

Crystallization encompasses the whole process, from the disentanglement and conformational change of the chains in amorphous region to the final formation of the ordered structure. During crystallization, flexible macromolecules can fold back and reenter in the same crystal to form a single lamellae. Crystals can be connected through tie chains or entanglements in the amorphous phase.
Crystallization starts with nucleation and proceeds with the growth mechanism. Favorable arrangement of the chain segments or the presence of external surfaces, including impurities or catalyst residues in the polymer melt, are considered the starting point of the homogeneous and heterogeneous nucleation, respectively. A minimum nucleus size is required to overcome the extra surface energy, which is introduced by the new interface, to cross the energy barrier and gain a thermodynamically favorable driving force for the crystal growth.

$$\Delta G = \frac{4}{3}\pi r^3 \Delta G_v + 4\pi r^2 \sigma \tag{2.1}$$

ΔG represents the Gibbs free energy, ΔG_v denotes the bulk free energy, and σ stands for the surface energy of the aggregate. By increasing the radius of nuclei r and the introduction of a new surface, ΔG increases [11]. As the nuclei reaches the critical size, free energy starts to decrease, and crystal growth becomes energetically more favorable.
According to Lauritzen and Hoffman, crystal growth takes place by an attachment of the chain segment to the surface of the crystals, called secondary nucleation. Further segments will be attached to the previous segments through chain folding as one of the possible mechanisms. Repetition of these steps results in the crystal growth. The crystallization can be summarized in three regimes, schematically shown in Fig. 2.4.

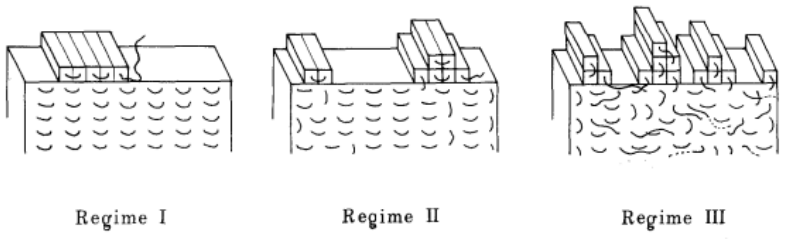

Figure 2.4: Schematic representation of three regimes of crystallization. Adapted and reproduced with permission: 1985, Springer Verlag [12].

In the first regime, the driving force for the nucleation is weak due to the low degree of the undercooling (difference between equilibrium melting temperature and crystallization temperature), and crystallization proceeds by attachment to the next segment. By decreasing the temperature, the rate of the nucleation exhibits a stronger increase compared to the growth rate. In the second regime, the rate of the nuclei formation on the crystal and the rate of the expansion of the crystal are close to each other, and both contribute to the crystallization process. In the third regime, due to the high undercooling, nucleation becomes

thermodynamically favorable, and the rate of nucleation outweighs the rate of crystal growth [13].
An interesting feature of PP is Polymorphism, which is the possibility of crystallization of the same polymer in different crystallographic structures, depending on the crystallization condition. In iPP, it results in the formation of stable α, metastable β or highly stable γ crystal forms. The monoclinic α form crystallizes from the melt under normal processing condition. α-PP has high stiffness and good thermal stability. Interesting for this form is the so called cross-hatching, where the α-form lamellae nucleate new lamellae through their side surfaces with an 81° angle between, creating a characteristic grid-like structure [14]. The studies on iPP show that the temperature gradient can influence the formation of the β-phase [15]. In the orthorhombic γ-form of iPP the polymer chains are not arranged parallel within the lamellae. The lamellae consist of bilayers, in which parallel helices in each bilayer are tilted about 80° relative to the adjacent layer [16]. The amount of the γ phase depends on the content of the co-units [17], chain irregularities and the presence of defects and their distribution. This form is characterized by increased stress at the yield point (for the same lamellar thickness) [18]. The presence of different polymorphic forms determines the physical and mechanical properties of the polymer [19]. Processing conditions such as cooling at a very high rate can lead to the formation of a mesomorphic form in iPP. During heating the mesophase transforms into the α-phase above 40°C.
Nucleating agents (NA) initiate the heterogeneous nucleation, create a high surface area, and lower the free energy barrier for the nuclei formation. One of the popular theories of heterogeneous nucleation states that for a given surface to act as a nucleant, there must be a lattice matching between the repetitive asperities on the NA surface and the distances between the methyl groups that form the asperities on the iPP crystal surface. Depending on the NA, it can nucleate the same crystallographic form of iPP via different crystallographic planes or different crystallographic forms (usually α and β). This influences the morphology and properties of iPP by mainly promoting the formation of thermodynamically stable polymorphic structure [20]. Using NA is an economic way to modify the mechanical and optical properties of the polymer. They can trigger some morphological changes in polymer by accelerating the crystallization process, increasing the crystallization temperature and melting temperature. Energy barrier for nucleation facilitates the study of the kinetics of the crystallization by cooling of the polymer melt without crystallization. Depending on the time and temperature, the crystals form and develop in the polymer melt. Avrami is one of the mathematical models to study the primary nucleation and crystal growth under isothermal crystallization condition. This model expresses the relation between the rate of conversion α during phase transition from liquid to solid, time of the crystallization t, as follows:

$$\alpha(t) = 1 - exp(-kt^n) \tag{2.2}$$

Plotting the logarithmic properties of this equation, provides information on dimensionality of the aggregates n and the constant rate of the crystal growth k

[13].

2.1.4 Thermal conductivity

Many polymers exhibit low thermal conductivity. This leads to weak heat dissipation, longer processing time above their melting temperature, and slowing down the cooling process, especially for bulky samples, which can significantly influence the physical properties. At the microscopic level, the mechanism of heat conduction in a solid state can be understood through correlated movement of lattice vibration via phonons. In the semicrystalline polymers, phonon transport occurs through molecular vibrations. Phonon scattering can be caused by the presence of defects and impurities, as well as phase boundaries within the material, or interaction with other phonons. This limits the pathway of phonons and can be contributed to the form of thermal resistance within the material [21].
Thermal conductivity K and the main factors that can highly influence it can be described by the Debye equation:

$$K = \frac{1}{3} C_v \cdot u \cdot L \tag{2.3}$$

C_v represents the specific heat capacity, u stands for the speed at which the phonon travels, and L is the distance that a phonon travels before getting scattered, respectively [22].
The semicrystalline polymer can be regarded as a composite consisting of two different phases. Generally, the strong bonds in the polymer backbone can provide a passage for the phonons. The higher chain length and a lower amount of side chains can result in an increase in the mean free pathway of the phonon [6]. Nevertheless, the thermal conductivity of bulk polymer exhibits a lower value than theoretical calculations suggest. Additionally, a higher amount of side chains can also affect the crystallinity and potentially cause a decrease in the lamellar thickness.
It has been found that highly ordered and aligned molecular chains within crystalline region can provide better heat transport compared to the amorphous region with disordered structure [23] [22]. It can be concluded that the polymers with a higher volume of the crystalline region can exhibit a higher thermal conductivity [24]. Furthermore, various orientations of the chains caused by an axial stretch of the material can enhance the phonon propagation in the drawing direction, but negatively influence the overall thermal conductivity of the material [25]. Improvement of the thermal conductivity of polymers has been widely investigated, and studies have shown that using various types of fillers with high thermal conductivity is a potentially effective approach. Factors such as the amount of filler, size, shape, and distribution of filler particles within the matrix, as well as thermal resistance at the filler/ polymer interface, can have a crucial impact on the thermal conductivity of the polymer. Some studies suggest that an optimal amount of thermally conductive filler in a polymer matrix can form an interconnected conductive pathway, which can enhance the thermal conductivity of the polymer [26]. The effect of interfacial resistance, which is a result of acoustic impedance mismatch of two phases, can lead to phonon scattering and thermal

resistance at the interface. This can be mitigated by surface modification [27][26][21]. Polymer composites can provide a solution to improve both the thermal conductivity and mechanical properties of the polymer. Depending on the chemical structure of the polymer and filler, the strong bond between the main chains or through the functional groups (crosslinking) can facilitate the propagation of phonons, by increasing the mean free path. However, a study on the effect of crosslinking on the thermal properties of a semicrystalline material reported that the crystallinity may exhibit a greater influence than the degree of crosslinking [28].

2.1.5 Mechanical properties

In polyolefins, crystallization time, cooling rate, and tacticity, influence the crystal structure, and the microstructure highly affect the physical properties of the polymer. In semicrystalline polymers, yield can be described as an irreversible breakdown or reorganization of the crystalline region. The mechanical behavior of a polymer depends on the stress-transfer mechanisms between the amorphous and crystalline phases. Tie chains can fold back to the crystals, entangle with other chains in the amorphous domain or directly link the crystalline lamellae, regulating the stress transfer and deformation of both phases. The amorphous phase plays an important role in the deformation process and can influence the deformation of the crystalline lamellae [29]. The plastic deformation of semicrystalline polymer involves the deformation of the amorphous region. In this process, crystal lamellae slide over each other, which is accompanied by an increase in interlamellar distance and rotation of lamellae stacks. At higher strains, lamellae undergo plastic deformation through various mechanisms including rotation and sliding, and additional processes until the lamellar crystal layers begin to break through micronecking, consequently forming microfibrils [30][31][32]. High crystalline polyolefins exhibit high stiffness and poor toughness at low temperature, which can be caused by the big size of the lamellae and the lack of stress transmitters between the lamellae, respectively. Single iPP crystallites in lamellar form usually organize into spherulitic polycrystalline aggregates, and their size may also affect the mechanical properties of the polymer. The lack of tie chains and segregation of impurities at the spherulite boundary may lead to brittle behavior and fracture in this region.

2.2 Additives

2.2.1 Liquid Additive A

LA.A is a viscous liquid with lubricating properties, It is chemically stable and suitable for use as a processing aid and protective medium in thermoplastic materials and other technical applications.

2.2.2 Liquid Additive B

Liquid additive B is a plasticizer. Plasticizers are low MW compounds with low volatility that in addition to the polymer, lowers the resistance of the material to deformation and depresses T_g of the polymer. Depending on the polymeric system they may be added as lubricants, but in different amount.

2.2.3 Liquid Additive C

Additive C is a base organic compound used as antioxidant.

2.2.4 Liquid Additive D

Additive D is a viscous liquid with lubricating function, suitable for thermoplastic material.

2.2.5 Liquid Additive E

Having a high viscosity index is an important requirement for a lubrication oil and the material shows a slower thinning behavior at higher temperatures. Additive E is a saturated hydrocarbons, which is known as a polymer modifier for thermoplastic polyolefins with lubricating function.

2.2.6 Liquid Additive F

Additive F is a viscous organic liquid antioxidant which, beside its antioxidant property, plays an important role in polymer processing to achieve an optimal MFI and a desired color. Due to its high stability, its application is extended to pharmaceutical and food packaging.

2.2.7 Liquid Additive H

Additive H is a vegetable oil. As a bio-based plasticizer, its application in plastic industry has been extensively studied.

2.2.8 Solid Additive I

The antioxidant I is one of the common additives in polymer industry. They can be introduced to the polymer in compounding process. By stabilizing polymer against oxidative degradation and improving its heat resistance, they enhance its service life. SA.I is a solid antioxidant that is also known for its heat stabilizing effect.

2.2.9 Solid Additive K

Additive K is a copolymer of iPP and randomly distributed ethylene unit. The distribution of the co-units is determined by the product of the reactivity of both monomers, which for random copolymer is close to 1 [33]. The stereoregularity of the iPP can be controlled by a suitable catalyst that leads to an improvement of the crystallinity.

2.2.10 Liquid Additive M

Additive M is an ester-based mineral oil. It is synthesized through the esterification of polyols and fatty acids and contains various antioxidants that ensure its high oxidation stability. According to manufacturer, the lack of ionic salts in its composition and the preservation condition under the nitrogen-blanketed atmosphere limit the risk of an increase in its water content.

2.2.11 Liquid Additive N

Some of the material properties including mechanical and thermal properties are influenced by MW of the polymer. Addition of chain transfer agent is a way to control the MW during polymerization and additive N is commonly used in polystyrene polymerization.

2.2.12 Solid Additive P

Additive P is a low molecular weight polymer, which is applied as plasticizer in plastic industry.

2.3 Analyzing methods

2.3.1 Thermogravimetric Analysis (TGA)

Thermogravimetric Analysis (TGA) is a thermal analysis method that allows the determination of the thermal stability of the materials. The measurements can be performed isothermally or non-isothermally [24]. The test setup comprises a balance for weight measurement, a heating furnace, a temperature control program, and a data recording system. The test can be performed under an inert N_2 or an oxidative environment. The weight loss or weight gain of the sample as the temperature increases will be recorded, and a transition on thermogram is an indication of vaporization followed by degradation of the sample or oxidation of the components [34]. By coupling an additional instrument, such as FTIR, with TGA the chemical information on emitted gas during the material decomposition can be collected and analyzed.
Basically, a minimum change in thermal stability at processing temperature upon additive incorporation is desired.

2.3.2 Fourier Transform Infrared Spectroscopy (FTIR)

Fourier transform infrared spectroscopy (FTIR) is an analysis technique that facilitates the study of the material's structure based on its absorption spectra in the infrared region. It helps to provide chemical information on infrared active substances and allows quick qualitative and quantitative measurements [35]. The ATR mode is commonly applied for the surface analysis. In this mode, infrared light is directed to the instrument's crystal at an angle greater than the critical angle. The light undergoes several reflections within the crystal, and a part of the energy is absorbed because of the interaction and propagation of the evanescent

wave in a small dept within the sample. The intensity of the light at frequencies that match the absorption bands of the sample is reduced and will be recorded. The absorbance at the specific wavelengths is characteristic of the material's structure.
It is a common approach to study the intramolecular interaction by detecting chemical bonds or functional groups and their corresponding vibration. In the polymer industry, FTIR, along with complementary techniques, can be used to gain a deeper insight into the variations in spatial distribution [36] in materials that are induced by the interaction with modifiers or by processing conditions that help evaluate the extent of their influence on the material properties [35][37]. The intermolecular interaction between the components or phases can be analyzed through the shifts or changes in the peaks on the spectrum [38][39]. In transmission mode, the infrared light is directed through the sample and the absorbance spectra will be recorded. Some factors can limit the application of this method, particularly in complex systems. The factors such as the nonuniform composition of the sample can complicate the spectra interpretation or interaction with the ambient conditions that lead to a change in the material's behavior or its properties [40]. In ATR mode, the depth of penetration of the evanescent wave d_p is determined by the wavelength of the IR light λ, angle of IR light θ and the refractive indices of both the material n_2 and the crystal n_1 [37].

$$d_p = \frac{\lambda}{2\pi n_1 \sqrt{\sin^2\theta - \left(\frac{n_2}{n_1}\right)^2}} \tag{2.4}$$

The quantitative evaluation can be performed using Beer-Lambert law in transmission mode. Absorbance A of sample follows the equation:

$$A = \varepsilon c \iota \tag{2.5}$$

ε, c, and ι represent molar absorption coefficient, concentration, and path length of sample, respectively.

2.3.3 Differential Scanning Calorimetry (DSC)

Differential scanning calorimetry (DSC) is a thermal analysis technique to determine the phase transition temperature and the associated change in enthalpy in the semicrystalline polymers and to evaluate their variation as a result of additive incorporation.
DSC instrument allows measurement based on power compensation and heat flux method. The principle of power compensating DSC involves maintaining the sample and reference at the same temperature, and the power is adjusted during the process. The difference in heat flow reflects the enthalpy change, and it is detectable as a peak on the DSC thermogram [41][34]. DSC provides easy sample preparation and fast measurement to study melting temperature T_m and crystallization temperature T_c, crystallinity, Glass transition temperature T_g or kinetics of crystallization by the measurement of enthalpy as a function of time or temperature [42]. The variations in the melting temperature or crystallization can

be used to study the changes in the crystalline properties of the polymer [41]. Filler could have an impact on the kinetics of crystallization by speeding up or slowing down the crystallization rate and altering the microstructure of the polymer. These variations can be screened by DSC [43]. Data analyzing and quantification are mainly based on the shape of the thermal curves and position of the peaks, but it can lead to complications, particularly for the overlapping peaks. These are two main challenges of this technique [44]. The difference in heat flow between the sample and the reference is measured by instrument.

$$\Delta Q = C\Delta T = c \cdot m \cdot \Delta T \tag{2.6}$$

Difference in heat flow Q, change in temperature ΔT, m is the mass of the sample, and c represents the specific heat capacity $c = \frac{C}{m}$.
The specific heat capacity reflects the material properties such as stability and order [44].

2.3.4 Transient Plane Source (TPS)

Transient plane source (TPS) is a method to measure the thermal conductivity of polymeric materials as the main heat transport mechanism. The transient method can provide information on how much and how fast heat waves can travel into the material. In comparison with the steady-state method, it is a quick and reliable method with minimal temperature fluctuations. A thin electrically insulated sensor with a double spiral wire pattern will be placed vertically or horizontally between two solid samples or within a liquid material, respectively. Heat pulses will be applied to the material through the sensor, which act as the source of heat and temperature sensor. The changes in resistance of the sensor are recorded over time. The thermal properties can be determined by fitting the data to a theoretical model. The higher temperature change reflects the higher thermal resistance of the surrounding material and a lower thermal conductivity [45].
Fleischner and Arzoha [46] have studied the criteria under which the thermal conductivity measurements in liquids can be negatively affected. This study highlights that a long measurement and applying a high heat power can lead to inaccuracy of the results. The thickness of the test material is an important factor that needs to be considered during the test and the sample preparation. A suitable sample thickness, together with a good surface contact with the sensor, can improve the accuracy of the measurement.
The distance Δp that the heat can travel into the material is related to the κ constant, which reflects the sensitivity of the temperature measurements, thermal diffusivity α and the duration of the test t is expressed by the following equation:

$$\Delta p = \kappa\sqrt{\alpha \cdot t} \tag{2.7}$$

During measurement, the temperature increase includes the temperature change at the surface of the sample T_S and the temperature variation across the testing sample T_i. It can be described as follows:

$$\Delta T = \Delta T_i + \Delta T_S \tag{2.8}$$

$$\Delta T = \Delta T_i + \frac{p_o}{\pi^{3/2} r \lambda} D(\tau) \tag{2.9}$$

p_o, r and λ represent the power output, the radius of the largest wire ring of the sensor, and the thermal conductivity of the test sample, respectively. $D(\tau)$ is a mathematical function. [47].

2.3.5 X-Ray Scattering

X-ray scattering allows the measurement of distances between different density regions for different length scales in polymer. Wide angle x-ray scattering (WAXS) is a characterization technique that allows for determining distances of the order of several angstroms. It enables the identification of different crystallographic forms in polymers, whereas small angle x-ray scattering (SAXS) facilitates the study of the thickness of lamellae within the nanometer range [48]. In this technique, a narrow X-ray beam travels through the sample and goes through several scattering on atoms, and the scattering angle depends on the distances between atoms. Depending on the repeatable distance between atoms, at a specific angle, the scattered light will be in phase (constructive interference), resulting in a maximum intensity. During the measurement, the scattering intensity as a function of scattering angle 2θ will be recorded [48][49]. The X-ray scattered at a small angle provides information regarding spacing between lamellae stacks and possibly volume crystallinity while the WAXS will be used to analyze the crystalline structure, including unit cell, crystallinity, and crystal size in some directions [49]. This method can provide insight into the localization of the noncrystallizable additives in the polymer blend. This amorphous component can be placed in interlamellar and/or intraspherulitic regions [50]. Bragg's law relates the distance between the lattice planes l_p to the scattering angel θ. λ represents the wavelength of X-ray beam and q stands for scattering vector.

$$q = \frac{2\pi}{l_p} = \frac{4\pi}{\lambda} Sin\theta \tag{2.10}$$

The long period and the crystalline volume fraction can be applied to estimate the lamellar thickness [48].

2.3.6 Mechanical Testing

In the evaluation of mechanical properties, the tensile test is commonly used to analyze the strength of the material and its deformation behavior. The material's response to the applied stress, at a constant strain rate will be recorded as a stress-strain curve. At a very low strain, there is a linear relationship between stress and strain and the deformation will be reversible. By increasing strain, material may fracture and exhibit a brittle behavior or a transition from elastic behavior to plastic behavior. The stress-strain curve can show a local maximum that indicates the onset of irreversible deformation of the material, which is known as the yield point. Evaluation of the stress-strain curve, at the point of failure provides information about the strength of the material [51][52]. The stress σ, is defined as the ratio of

the force F to the cross section A_0 of the specimen.

$$\sigma = \frac{F}{A_0} \tag{2.11}$$

The strain ε, is defined as the ratio of the change in the length of the specimen to its initial length l_0.

$$\varepsilon = (\frac{\iota - \iota_0}{\iota_0}) = \frac{\Delta\iota}{\iota_0} \tag{2.12}$$

The Young's modulus indicates how hard a material deforms within its elastic range. The constant E is from Hooke's law. It is defined as:

$$\sigma = \varepsilon E \tag{2.13}$$

The elongation at break and the stress at break are defined as the amount of strain and stress at the breaking point of a material, respectively [51].

2.3.7 Dynamic Mechanical Thermal Analysis

Dynamic mechanical analysis (DMTA) is a mechanical characterization technique to study the viscoelastic behavior of polymeric materials. In this method, a constant sinusoidal stress is applied to the material, and its deformation is recorded as the temperature increases. Depending on the material behavior, stress and strain can be in-phase interpreted as an elastic behavior or out of phase, with 90 degree phase lag, and exhibit a purely viscous behavior. Analyzing the shape of the DMA curve of the materials can provide an estimation of the degree of crystallinity or crosslinking of the semicrystalline material [52]. At low temperatures, the movements of the chains are limited, but by increasing temperature, the movement of the side chains, and at a higher temperature, mobility of the larger segments in the main chain becomes activated, and these changes can be seen as several transitions in a thermogram. T_g represents the temperature at which chain movements in the amorphous phase start. It is important information that highly depends on the test conditions, such as heating rate, applied frequency, and stress or strain. Any variation in the T_g can be attributed to the changes in the amorphous phase, such as interfacial interaction between the filler and the polymer, pointing to the changes in the mechanical properties [53][54][39]. According to previous studies, the geometry, size, concentration, and distribution of the filler can influence the polymer properties [54]. The miscibility of two components at a molecular level can be inferred from the presence of a single T_g; otherwise two separated T_gs may suggest the phase separation in the system.

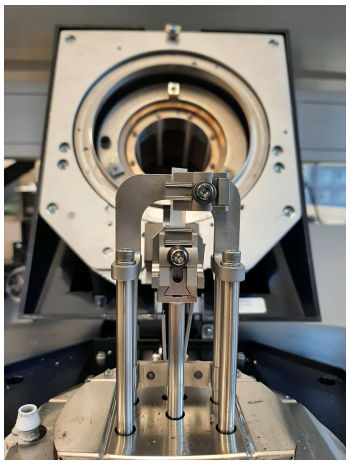

Figure 2.5: Sample fixed between clamps of DMA

This method provides information on the storage or dissipation of energy in the material as a result of applied stress. Storage modulus E' and loss modulus E'' represent the material response to stress, and are calculated as follows:

$$E' = E_0 \cos(\delta) \tag{2.14}$$

$$E'' = E_0 \sin(\delta) \tag{2.15}$$

E_0 represents the strain value by applying maximum stress, while δ represents the phase difference between applied stress and strain.
Tan delta, as the ratio of loss modulus to storage modulus can be described as follows [53]:

$$\tan \delta = \frac{E''}{E'} \tag{2.16}$$

3
Methods

For all experiments heterophasic PP copolymer (NP) was used. NP and pre-blended pellets (polymer blends) containing various liquid additives (LA) and solid additives (SA) in different concentrations were used for the experiments. Starting from these polymer blends were either plaques or tapes prepared to study the blends using different techniques. Plaques and tapes of different thicknesses were prepared to perform the thermal conductivity, saturation concentration, FTIR, tensile, small angle X-ray scattering (SAXS), wide angle X-ray scattering (WAXS) and thermo-mechanical tests. The TGA test method was performed to examine the thermal stability of the additives and polymer blends during sample preparation. The influence of the additives on the degradation of the polymer was evaluated. The saturation concentration test was carried out to determine the upper limit of the additive incorporation into the NP to avoid phase separation. An exudation test on plaques was carried out to estimate the extent of the migration of additives to the surface at elevated temperature over time. To quantify the additive content in the polymer blends, the FTIR technique was carried out. The DSC thermo analysis technique was conducted to determine the crystalline mass fraction of the samples, evaluate the changes in the melting temperature, and compare the effect of two sample preparation methods. WAXS analysis was carried out on samples prepared by compression molding and tape extrusion methods to qualitatively investigate the crystallographic forms present in the samples and to evaluate their variations caused by two sample preparation methods. The variations in the kinetics of crystallization, including nucleation and growth mechanisms upon additive incorporation were also studied with DSC.
The TPS method was used to evaluate the thermal conductivity of the polymer blends as a result of additive incorporation into the polymer. SAXS analysis was performed to study the lamellar structure. The potential changes in the lamellar thickness, and the interlamellar distance as a result of LA incorporation were investigated. To examine the variations in tensile modulus and yield stress of the samples, the tensile test was performed. DMA test was performed to study behavior (performance) of the material in a wide temperature range and evaluate the potential change in the glass transition temperatures.

3.1 Compounding

NP pellets were extruded with various concentrations of additives within a processing temperature range of 200-220°C. To ensure homogeneous blending, a

twin screw extruder was used. Polymer blends are listed in Table 3.1.

Table 3.1: List of Polymer blends

Abbreviation	Description
NP	Heterphasic PP copolymer
P.A1%	polymer blend with 1% liquid additive A
P.A3%	polymer blend with 3% liquid additive A
P.A6%	polymer blend with 6% liquid additive A
P.B1%	polymer blend with 1% liquid additive B
P.C1%	polymer blend with 1% liquid additive C
P.C3%	polymer blend with 3% liquid additive C
P.D1%	polymer blend with 1% liquid additive D
P.E1%	polymer blend with 1% liquid additive E
P.E3%	polymer blend with 3% liquid additive E
P.F1%	polymer blend with 1% liquid additive F
P.H1%	polymer blend with 1% liquid additive H
P.I1%	polymer blend with 1% solid additive I
P.I3%	polymer blend with 3% solid additive I
P.K1%	polymer blend with 1% solid additive K
P.K3%	polymer blend with 3% solid additive K
P.N1%	polymer blend with 1% liquid additive N
P.P1%	polymer blend with 1% solid additive P
P.P3%	polymer blend with 3% solid additive P

3.1.1 Addition

Two separate batches of P.M3% and P.B3% pellets were prepared by addition of LA.M and LA.B at elevated temperature, as they were not available in compounded form. In this method, NP pellets were preheated at 60°C in an oven for 8 hours, subsequently mixed with LAs in a weight ratio of 97% to 3%, and heated in a small carousel oven at 60°C. The liquid uptake was optically controlled at 30-minute intervals to reach full absorption in a minimum time and to avoid the fracture of the pellets. As shown in Fig. 3.1 P.M3% did not show a full absorption of the additive even after 6 hours impregnation. This step is followed by a ripening at 60°C for 12 hours. Pellets were used for the preparation of samples for the FTIR test.

Figure 3.1: P.M3% after 6 hours impregnation

3.2 Thermogravimetry

The analysis was performed using TGA/DSC 3^+ instrument on LAs, neat polymer (NP) and the pre-blended pellets (polymer blends) in approximately 8 mg, weighed in an alumina crucible. Measurements were made in a temperature range of 30 to 400°C under N_2 gas at a flow rate of 60 mLmin^{-1} and heating rate of 10 Kmin^{-1}. This test was performed to study the thermal stability of the LAs and the polymer blends under processing condition.

3.3 Saturation Concentration/ Exudation Test

NP plaques with a thickness of 1 mm were punched in dumbbell-shape specimens (5A specimens) using a manual cutting machine. As illustrated in Fig. 3.2, samples were submerged in LAs and preserved in the oven at 60°C for 340 hours. NP specimen, used as a reference, was also placed in the oven under the same condition to control the changes in its properties over time. The weight change of the samples was recorded at various intervals using METTLERTOLEDO analytical balance with an accuracy of ±0,01 mg. Before each measurement, samples were dried with a tissue without applying pressure. For exudation test, plaques in 4 mm-thickness were kept in oven at 60°C for 340 hours, wiped off and the weight loss of the samples was recorded over time.

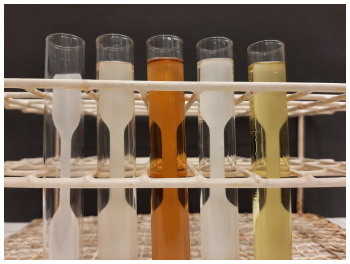

Figure 3.2: NP without LA, NP specimens submerged in LA.H, LA.F, LA.M and LA.C.

3.4 Fourier Transform Infrared Spectroscopy

FTIR spectra for the NP, additives, and polymer blends were recorded in transmission mode at a resolution of 4 cm^{-1} and 16 scans, in mid-infrared region 4000-450 cm^{-1}, using a BRUKER Invenio-S instrument. FTIR spectra in ATR mode for P.E, P.A and LAs were recorded under the same conditions, using a PerkinElmer instrument. In this method, to achieve better contact with the crystal of the instrument, the sample was fixed with the metal arm of the instrument.
In both methods background spectra were recorded prior to the measurements to eliminate the effect of the atmospheric interferences. In ATR mode, quantitative measurement of the additive content in blended samples was calculated by the absorbance ratio (the hight of the peak) of the blend relative to that of the NP

after normalization. Due to the presence of similar peaks in polymer blends P.E and P.A compared to NP, the peak at 899 cm^{-1}, with an increasing trend in the signal intensity was selected. It appears that this trend can be caused by different amounts of additives in the polymer blend. The ratio of the difference in the peak hight relative to the peak intensity at the same peak for NP was calculated and reported. For the blends with the new peak resulting from the additive, the peak area of the new peak was used for the calculation. The additives were diluted in a CS_2 solution, and their spectra were recorded using NaCl liquid cell. It was assumed that the molar absorptivity ε of a highly diluted additive (5% concentration) is equal to that of the thin plaque of polymer blend. The volumetric amount of the additive in polymer blends was calculated with the known concentration values for diluted additive. The absorbance value was determined based on the peak area. The Beer-lambert law was used for the calculation:

$$\frac{A_1}{A_2} = \frac{\varepsilon_1 c_1 \iota_1}{\varepsilon_2 c_2 \iota_2} \tag{3.1}$$

A represents the absorbance, ϵ stands for molar extinction coefficient and c and l represent concentration and path length of light in the medium, respectively. The thicknesses of the liquid cell 0,107 mm, NP and the polymer blend were known.

3.5 Sample Preparation

3.5.1 Tape Extrusion

Compounded pellets from the previous stage, were extruded into tapes using a Collin Teach-Line E-20T tape extruder. The extruder with a manual feeding system consists of a 20x25 mm screw and several heating zones. The speed of the screw controls the feeding rate and together with various temperatures of the barrel, ensures compression, melting and mixing of the material in transition and metering zones, respectively. The material is processed into a homogeneous liquid melt, subsequently drawn, and guided through a 2 mm flat nozzle at the outlet by various rollers. The adjustable speed of the rollers allowed to provide tapes in a range of 1,8-2 mm thickness. The tape was cooled to room temperature by exposure to an adjustable air stream. At the end of the line an automatic trimmer cuts the tapes to a specific length. Tapes in 1,8 to 2 mm thickness were prepared for a tensile test.

3.5.2 Compression Molding

Blends of polymer and additives were used to prepare plaques in 0,3, 1 mm, and 4 mm with Hotpress Fontijne. The samples were placed in a hot press at the temperature range of 200-220°C to melt, compressed, and then cooled down at a rate of 15 $°Cmin^{-1}$ to room temperature. 0,3 mm samples were used for DMTA, for mechanical test, as well as for the SAXS test. plaques in 1 mm thickness were used for saturation concentration test. 4 mm samples were prepared with the same temperature program and using the Collin P 400 P/M instrument. These samples were used for thermal conductivity test.

3.6 Differential Scanning Calorimetry

The plaques, tapes and saturation concentration test samples were analyzed using a METTLER TOLEDO DSC5$^+$ instrument in power compensation mode. The analysis was performed under N_2 gas at a flow rate of 60 mLmin^{-1}. The samples weighed in a range of 8-9 mg, sealed in an aluminum crucible, were subjected to predefined heating, isothermal, and cooling cycles with the heating/cooling rate of 10 Kmin^{-1}, between -40 and 200°C. The crystalline mass fraction was calculated solely based on the polymer content, reflecting the crystallinity of the polymer in the blends. The enthalpies were calculated from the peak area within a fixed temperature range for all the samples. The data collected from the first heating step was used for the evaluations.
The crystalline mass fraction X of PP is calculated as follows:

$$X = \frac{\Delta H_{\mathrm{m}}}{a\Delta H^0_{\mathrm{m}}} \tag{3.2}$$

ΔH_{m} represents the melting enthalpy of the sample and ΔH^0_{m} the enthalpy of fully crystalline polymer [41] and a stands for the amount of NP in blend(%). The value of ΔH^0_{m} for the fully crystalline polymer is assumed to be 209 Jg^{-1}.
The saturated samples from saturation concentration test were analyzed using a DSC instrument to investigate the degree of crystallinity and change in the melting temperature.
To understand the possible differences in crystallization of polymer due to additive incorporation, the kinetics of crystallization was studied. Samples of NP 5-6 mg, sealed in aluminum crucible, were analyzed under N_2 gas at a flow rate of 50 mLmin^{-1}. NP pellet was heated from 30 to 200°C with a heating rate of 10 Kmin^{-1}, followed by an isothermal step for 5 min at 200°C, then cooling at a rate of 10 Kmin^{-1} to 130°C. To verify the optimal crystallization temperature, a temperature range of 120 to 130°C was selected, and an isothermal crystallization at 130°C was conducted on NP and P.A. Measurement error was assessed by performing random three measurements on some samples and comparison between the results from CM and TE. Errors for X and T were found to be 0,01 and ±1°C, respectively.

3.7 Transient Plane Source

Melt compression molded Plaques with 4 mm thickness were analyzed using Hot Disk® TPS2500s instrument for isotropic sample. To measure the thermal conductivity of the SAs, plaques each 3-4 mm-thickness, were prepared with the standard thermal program cycles using Hotpress Fontijne instrument. Due to the viscous-adhesive nature of the SA.I, measurement of the thermal conductivity was not possible. The 5465 (3,2 mm) sensor was used for NP, the polymer blends, and the SA plaques with a measurement time of 40 s and a heating power of 30 mW. For LA samples, the 7577 (2 mm) sensor was used with a measurement time of 5 s, and a heating power of 35 mW. The variations in thermal conductivity of samples

as a result of additive incorporation into the polymer were analyzed. To achieve a smooth surface and maximal contact between the sample and the sensor, the surface of the plaques was polished. From each material, two replicates were taken and a total of 10 measurements were performed. Measurement accuracy was assumed to be 5% in accordance with the standard ISO 22007-2:2015.

3.8 Small Angle X-Ray Scattering

Plaques approximately 1 mm thick, prepared by compression molding, were tested using Mat: Nordic instrument from SAXSLAB/Xenocs. A Dectris Pilatus 300K detector was coupled to a microfocus CuK_α beam line (λ= 1,54 Å). The test was conducted to measure and compare the lamellar thickness in polymer blends against that of the NP. Each measurement was performed for one hour. The SAXSGui software was used for data evaluation. Long period l_p, which indicates the thickness of the lamellae and the amorphous phase adjacent to it, was determined from the scattering vector q on diffractogram.

$$l_p = \frac{2\pi}{q} \tag{3.3}$$

The lamellar thickness was calculated using long period value, crystalline mass fraction X_C, the density of the polymer blends ρ_s and the known density value of PP crystalline fraction ρ_c 0,946 gcm^{-3}.

$$l_c = l_p \times X_c \frac{\rho_s}{\rho_c} \tag{3.4}$$

The density of the polymer blends were determined using Isododecane with the known density values ρ_0=0,7469 gcm^{-3} and that for air ρ_l=0,0012 gcm^{-3}, according to the following equation:

$$\rho_s = \frac{A}{A-B}(\rho_0 - \rho_l) + \rho_l \tag{3.5}$$

A and B values represent the weight of the sample in Air and submerged in isododecane, respectively. The crystalline mass fraction of PP (X_c is calculated for the whole sample according to the following equation:

$$X_c = \frac{\Delta H_\mathrm{m}}{\Delta H^0_\mathrm{m}} \tag{3.6}$$

Measurement error for a long period was estimated based on the resolution of the detector used for the measurement equal to 2 Å, and accordingly calculated for the lamellar thickness that points to 1 Å. The error for ρ_s, is reported as standard deviation from two measurements.

3.9 Wide Angle X-Ray Scattering

The scattering pattern of the tapes and 4 mm thick samples prepared by compression molding, were recorded using a D8 Discover instrument from Brucker. The measurements were carried out in reflection mode, using a beam source of Cu$K\alpha$ (λ= 1,54 Å) and a constant slit mode 0,7 mm in a range of 10-70 degrees.

3.10 Mechanical Testing

Tapes, each 1,8-2 mm thick, prepared by tape extrusion, were punched into 5A specimens in the drawing direction using a hydraulic press, and their mechanical properties were tested using a Zwick Z010 instrument. The method was performed according to the standard ISO 527-1. The crosshead speed was adjusted to 25 mmmin^{-1}, and the gauge width and thickness of the specimens were approximately 4 mm and 1,8 mm, respectively. Tensile modulus, yield stress, elongation at break, and stress at break were recorded by instrument to evaluate the impact of the different liquids in varying concentrations on stiffness and strength of the material. The measurements were performed on six samples from each material, which were stored at 23°C, 50% RH for four days. The shape of the specimen is presented in Fig. 3.3. The standard deviation for six replicates was reported as the measurement error.

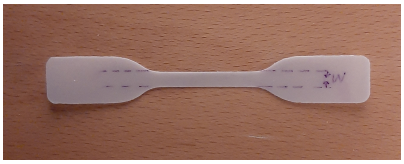

Figure 3.3: The Dumbbell-shape specimen (5A specimen) for tensile test.

3.11 Dynamic Mechanical Thermal Analysis

Plaques, each 0,3 mm thick, prepared by compression molding, were used for this analysis. DMA curves for the NP and blends were recorded in tensile mode. In this mode a constant frequency of 1.0 Hz was applied and a heating rate of 3,0 Kmin^{-1} was set over the temperature range of -80 to 190°C using DMA850 instrument. The initial force of 5 mN, 0,1% strain, and a clamp distance about 10 mm were set for the measurements. The values of the glass transition temperatures were obtained from the loss modulus curve. A single measurement was conducted on each polymer blend and a 10% error was reported for the measurement of the sample dimensions (cross section and thickness).

4

Results and Discussion

This part is divided into two sections. In the first section, the results of the material examination are presented. This section includes the thermal stability, saturation concentration test, FTIR spectroscopy, SAXS, DSC results on samples prepared by the CM and TE method, and WAXS, followed by the kinetics of the crystallization as primary studies of the polymer additive system. In the second part, the test results related to the material properties are presented. The results are discussed for thermal conductivity, and the mechanical testing.

4.1 Material Examination

4.1.1 Thermal Stability

4.1.1.1 Thermal Stability of the LAs and SAs

The thermal stability of the LAs and SAs within the processing temperature range of 200 to 220°C is an important criterion. The evaluation of the temperature at which the additive or polymer blend loses 5% of its initial weight can be considered the onset of degradation. As presented in Fig. 4.1, LA.N and LA.G start degrading at 189°C and 145°C, respectively. While other additives remain stable. These two additives have been excluded from the experiments. SA.K did not reach 95% of its initial weight even at 400°C.

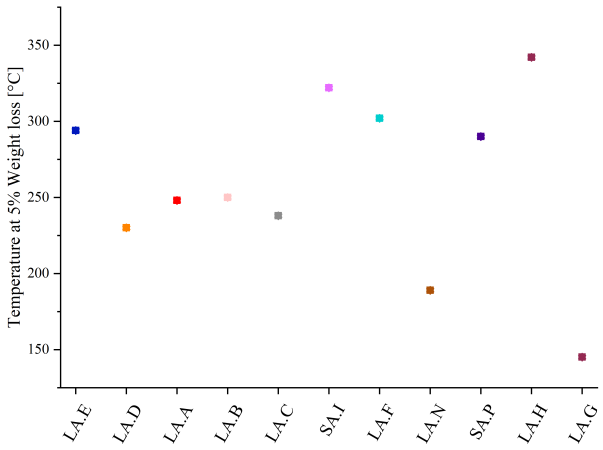

Figure 4.1: 5% decrease in the weight of LAs and SAs.

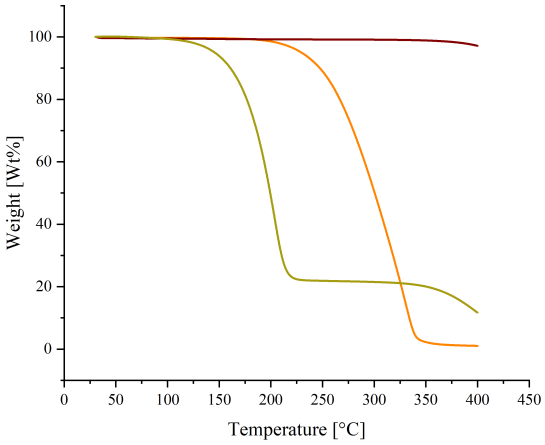

Figure 4.2: Weight% of LAs and SAs vs. Temperature. SA.K (dark brown curve), LA.D (orange curve), and LA.G (light green curve).

4.1.1.2 Thermal Stability of the Polymer Blends

Since additives or blending process may negatively affect the thermal stability of polymers, it was necessary to assess the blends in this respect. The polymer blends with the highest content of the additives were tested for thermal stability using a TGA instrument.
The results of weight loss at 400°C are presented in Fig. 4.3 and the corresponding curves for the NP, P.K3% and P.I3% are plotted in Fig. 4.4. Addition of liquid to NP reduces its thermal stability, although the effect is not strong and the weight loss for blends increases by maximum 5,3% at 400°C for P.A6%. At higher liquid content, additional stabilization of the polymer may be necessary. The polymer blends are stable within the processing temperature range of 200 to 220°C. The stability of the NP is less affected by the incorporation of 3% polymer modifier SA.K (P.K3%), while the introduction of the same amount of the antioxidant SA.I shows a higher effect on the stability of the polymer (P.I3%).

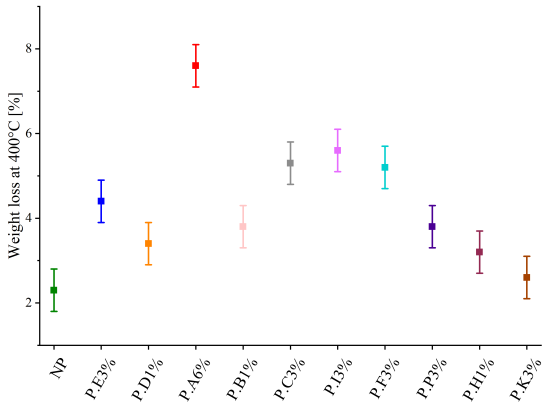

Figure 4.3: Weight loss% of NP and polymer blends at 400°C.

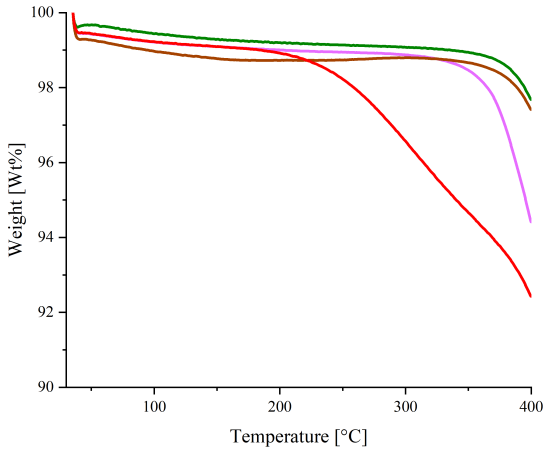

Figure 4.4: Weight% of the polymer blends vs. temperature. NP (green curve), P.K3% (dark brown curve), P.I3% (pink curve), and P.A6% (red curve).

4.1.2 Saturation Concentration Test

This test was conducted to determine to which extent liquid additive can be dispersed in the polymer system. The specimen submerged in LAs reached the maximum saturation at different amounts and at different times. As shown in Fig. 4.5, the specimen in LA.A shows the highest degree of swelling and, after 100 hours, reached an additive concentration of approximately 35%. Meanwhile, the specimen in LA.D with the lowest additive concentration showed a 4% weight increase after about 200 hours. The molecular size of the diffusant, viscosity together with the degree of swelling of the polymer and the interaction between two phases are the main factors that influence the diffusion.
Further study of the diffusion behavior to assign a diffusion model can provide an estimation for the diffusion coefficient and diffusion rate of the additives [55]. Having a high diffusion rate may promote a homogeneous distribution of the additive within the system. However, from another viewpoint, it may also accelerate the migration of the additive to the polymer surface. The exudation test did not suggest a change in the additive amount in the sample. For most of the samples, no exudation was observed after 340 hours. P.C%3 exhibited the highest amount of the additive migration to the surface, which was about 0,5%.

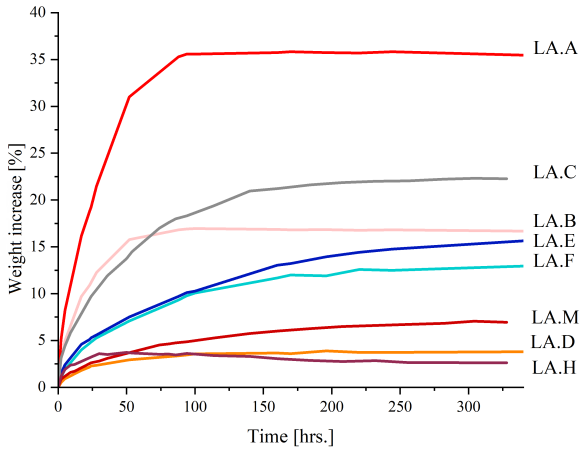

Figure 4.5: Weight increase vs. Time

To understand how the introduction of liquid affects the thermal properties of samples, DSC experiments on saturated samples were performed. The values of crystalline mass fraction X of PP, melting temperature T_m and crystallization temperature T_c from the DSC test on saturated samples are presented in Fig. 4.6 and Fig. 4.7. The values for X were determined as described in section 3.6, the T_m and T_c were obtained from the DSC-thermogram.
To avoid the influence of long term annealing on iPP secondary crystallization, the NP sample was annealed the same way for comparison. The lack of significant changes in crystalline mass fraction indicates that this parameter probably was not highly affected by the introduction of the liquid content. However, a small decrease in the melting enthalpy of the NP submerged in LA.H can be an indication of the strong interaction between them and possibly partial dissolution of the polymer, which could affect saturation concentration results. For most of

the samples, crystalline fraction remains fairly constant, and the melting temperature depression appears not to be solely attributed to it. The error measurement is described in section 3.6. The relationship between additive

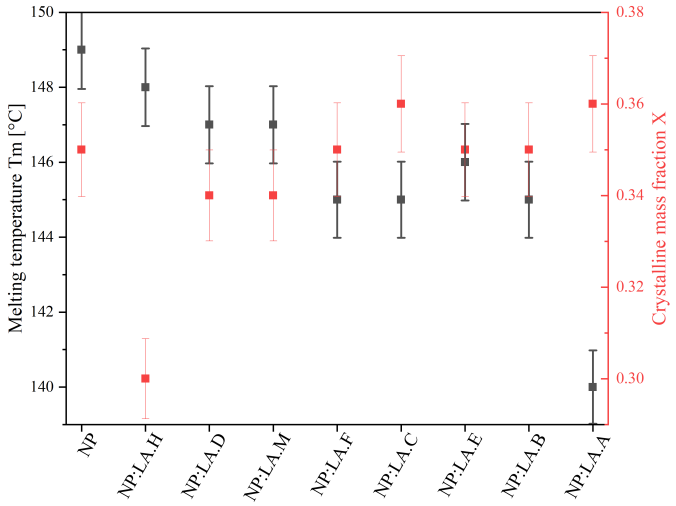

Figure 4.6: Melting temperature T_m and crystalline mass fraction X of NP after 340 hours of submersion in various LAs.

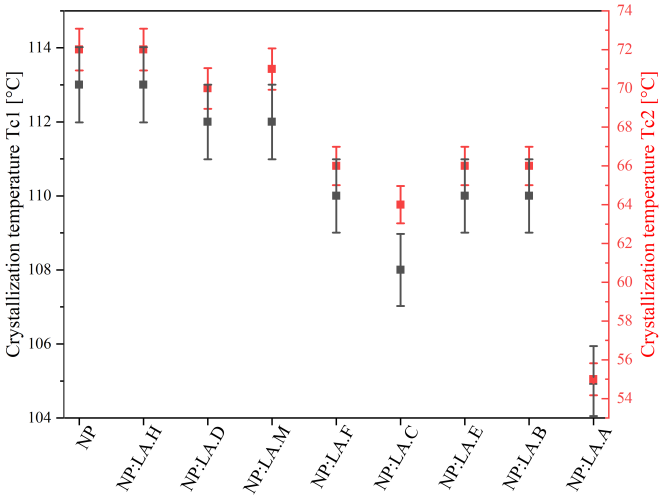

Figure 4.7: Crystallization temperatures T_c1 and T_c2 of NP after 340 hours of submersion in various LAs.

content, and melting point is shown in Fig. 4.8. It is observed that by increasing the concentration of the additive in the polymer blend, there is a decrease in the melting temperature. It appears that, regardless of the type of the additives, the melting temperature shows a dependency on the LA content.
Since X does not change with additive content during saturation test, we can assume that the decrease in melting point is not related to the change in lamellar thickness, and the liquids only cause swelling in the amorphous phase. The

presence of liquid in the amorphous phase depresses the melting point either by chemical interaction of the liquid with the polymer or by physically generating additional stresses on the crystals, which has already been described in the literature [41].
Additionally, this effect is accompanied by a decrease in the crystallization temperature recorded during DSC cooling. During cooling we can observe two separated peaks, one at a temperature close to 113°C related to the PP crystallization and the second peak at 72°C, which is most probably connected to the crystallization of the PE parts of chains in EPR. It was observed that the T_c of the PE in EPR phase is more influenced by the additive content (35%) and drops by $\Delta T_c 2 = 17$°C compared to PP in matrix which drops $\Delta T_c 1 = 8$°C. The melting

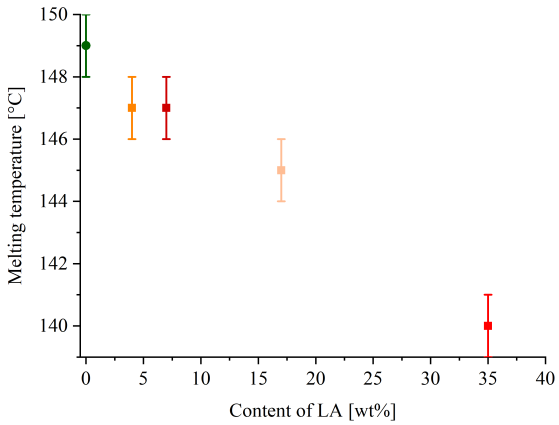

Figure 4.8: Melting point depression vs. LA content in NP. No LA (green pint), LA.D (orange point), LA.M (burgundy point), LA.B (light brown point), and LA.A (red point).

temperature depression can be accounted for by the thermodynamics of mixing. According to the Gibbs free energy of mixing $\Delta G = \Delta H - T\Delta S$ for a miscible system $\Delta G<0$. In a polymer- solvent system, entropy increases upon mixing, and the change in enthalpy, which is related to the interaction between two components, is decisive for miscibility. In the molten state, an additional energy is introduced into the system, which helps to decrease the attractive intramolecular forces in the polymer and solvent and promote an interaction between them. This may lead to an increase in the solubility and a decrease in the melting temperature. It would be interesting to study the variations in melting temperature for different volume fractions of polymer-solvent mixtures (phase diagram). Nishi and Wang [56] studied the strength of the interaction in a binary system based on the Flory-Huggins theory. This method accompanied with Hoffman-weeks analysis can provide details on the interaction in the system and provide an estimation for the equilibrium melting temperature, respectively.

4.1.3 Fourier Transform Infrared Spectroscopy

In order to assess the amount of additives in the plaques of polymer blends, the FTIR analysis was performed. The analysis of the spectra obtained from NP suggests several peaks at wave numbers 1166 cm^{-1}, 998 cm^{-1}, 974 cm^{-1} and 841 cm^{-1}, which are the characteristic peaks of semicrystalline iPP. As presented in Fig. 4.9, the recorded spectra of some polymer blends suggest the formation of new peak at the wave numbers ranging from 1740 to 1745 cm^{-1}. This new peak for P.H, P.D, P.M, P.I, and P.B was observed, and it can be related to the characteristic peak resulting from the free or dissolved carbonyl group of the additives in the polymer system.

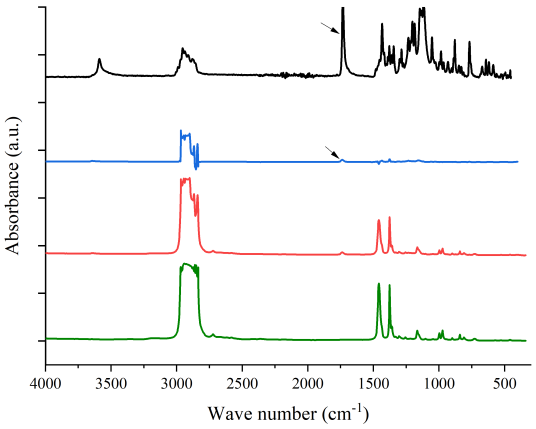

Figure 4.9: Comparison of absorbance spectra of NP (green) with P.I3% (red), subtraction of both spectras (blue) and spectra of SA.I (black).

The spectrum of P.E did not exhibit any additional peak compared to that of the NP, and Fig. 4.10 presents a comparison between the spectra of P.E1% relative to that of the NP. The lack of new peak in the P.E blend challenged the quantification

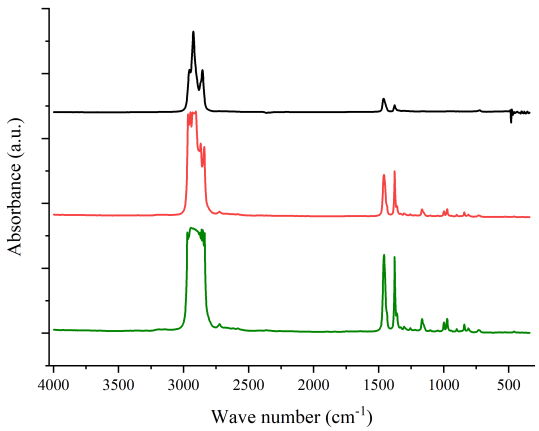

Figure 4.10: Comparison of absorbance spectra of NP (green) with P.E1% (red), subtraction (blue) and LA.E (black).

method. Quantitative evaluation of the P.E was carried out using ATR mode. Since

the LA peaks overlap with NP, the only way to calculate the amount of liquid in the blend was to use the NP-only peak and see how much it decreases in the blends. As explained in the method, the peak at 899 cm^{-1} was selected for the quantitative evaluation, and the calculated values are presented in Table 4.1. The amount of the additives looks overestimated. It appears that the applied pressure by the metal arm of the instrument may have caused the migration of liquid additive to the surface and resulted in an increase in the concentration of the liquid close to the surface. It was found that quantitative evaluation in ATR mode was unreliable. Comparing

Sample	**Additive content** [%]
P.E1%	3
P.E3%	7

Table 4.1: The additive content assessed using IR-spectra in ATR mode.

the spectra of the additive with the spectra from its blend and that of the NP; in almost all blends, the characteristic peak related to the additive is slightly shifted and some changes were observed in the shape of the peaks (peak shoulders). As explained previously, a new peak that resulted from the additive incorporation was observed in some blends. The recorded spectra for P.H, P.D, P.M, P.I, and P.B in transmission mode were used for the quantitative evaluation, using Beer-Lambert law. Based on our assumption, absorbance coefficient of the highly diluted LA was used for the quantification of the volumetric amount of the additives in the polymer blend. The quantified amount of the additives in the various plaques is presented in Table 4.2.

Sample	**Additive content** [%]
P.D1%	3
P.B1%	0,3
P.I1%	1,8
P.I3%	2,52
P.H1%	0,1
P.M3%	1,7

Table 4.2: The additive content assessed using IR-spectra in transmission mode using Beer-Lambert law.

The quantitative measurement of the blends with the various additive concentrations suggested the presence of a higher amount of additives in the blend. It can be concluded that the quantification of the additive directly from the spectra was not possible for the blends, and the values were unreliable.

4.1.4 Kinetics of Crystallization

The addition of liquid to polymer can cause changes in the nucleation and growth process of polymer crystals, which we observed through changes in the crystallization temperature of impregnated samples. To better understand this process, isothermal crystallization of NP and polymer blends was conducted at 130°C for one hour. Fig. 4.11 shows the heat flow curve of P.A3%, P.P3%, P.K3% and NP. It clearly presents the influence of the additive on the rate of crystallization. The same amount of various additives shifted the peaks of the crystallization curve differently. In

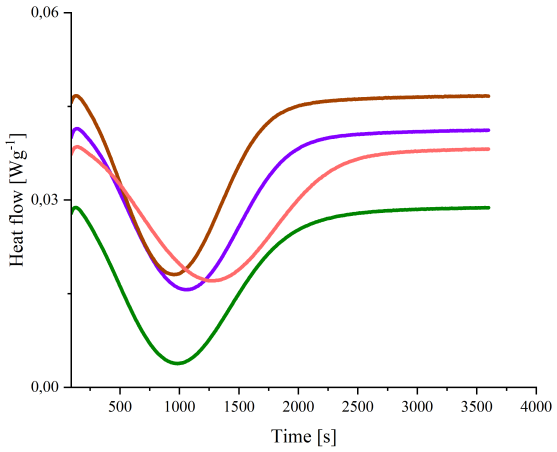

Figure 4.11: Heat flow curves as a function of time for P.K3%(brown curve), P.P3% (violet curve) and P.A3% (light red curve), NP(green curve). Isothermal crystallization at 130°C.

different blends, it was observed that the peak of crystallization in P.E1%, P.P1%, and the P.K blend at 1% and 3% was slightly shifted to an earlier time, while 1% of SA.I and LA.C did not exhibit a large influence on the time corresponding to the peak of crystallization. Overall, for most of samples, the crystallization slows down as a result of additive incorporation, and the peak of crystallization is shifted towards a longer time. The influence of the amount of LA.A on the rate of crystallization is presented in Fig. 4.12. A decrease in rate of crystallization upon the addition of additives was observed for all blends. The classical Avrami model is applied to analyze the crystallization process of NP and P.A under isothermal conditions. The degree of phase conversion, which reflects the extent of phase transition, is obtained from the DSC thermogram. The double logarithmic form of Avrami equation ln(-ln(1/1- α) for blends as a function of time ln(t) is presented in Fig. 4.13. As illustrated, the slope of the linear fitting slightly increases upon increasing additive content, and the intercept indicates a lower value compared to NP. Table 4.3 presents the calculated values for Avrami index n and the crystallization rate constant k for NP and P.A in conversion range between 3 and 20%. The value of n indicates a two-dimensional instantaneous nucleation, and the variations in the k value indicate a decrease in the rate of crystal growth. Small changes in n suggest a small influence of the liquid on the dimensionality of the growth of polycrystalline agglomerates and, therefore, on nucleation. Larger changes are visible for k, which suggests

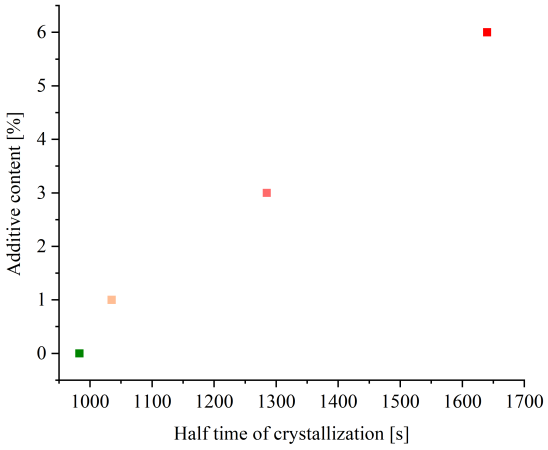

Figure 4.12: Additive content vs. Half time of crystallization. NP(green), P.A1% (light orange), P.A3% (light red), and P.A6% (red).

Sample	n	k	$t_{1/2}$
NP	2,37±0,001	-16,61±0,007	851
P.A1%	2,52±0,001	-17,68±0,007	901
P.A3%	2,48±0,002	-17,93±0,014	1140
P.A6%	2,47±0,003	-18,52±0,019	1501

Table 4.3: Isothermal crystallization parameters of NP, P.A1%, P.A3%, and P.A6%. Standard error for the linear fitting is reported.

differences in the rate of crystal growth. A study on nucleation of PP on PTFE fibers showed the similar n value [57]. It was observed that the values for n and k show a dependency on the selected interval for the degree of phase conversion α. However, obtained values in different intervals point to slight variations for n and a decrease in the k value upon additive inclusion. As the crystallization proceeds, the non-crystallizable component (additive) is pushed out of the growing crystal, and the ratio of the solvent to the polymer melt increases. It gradually becomes more difficult for the polymer chains to diffuse to the crystal surface, which results in a decrease in the rate of crystallization. The mathematical equation in Avrami model did not suggest the correct values for the half-time of crystallization and the peak of crystallization. It is likely that the assumption of constant crystal growth rate may not be true for blends with liquids. It would be interesting to investigate the growth rate and size of the crystal using polarized optical microscopy. These data may provide insight into the kinetics and the variations in the crystal size distribution.

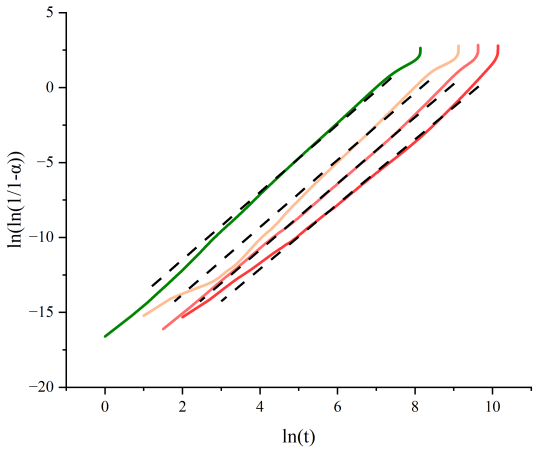

Figure 4.13: Plots of ln(-ln(1/1- α) vs. ln(t) for NP (green curve), P.A1% (light orange curve), P.A3% (light red curve), and P.A6% (red curve). The curves are vertically shifted for clarity and better illustration.

4.1.5 DSC of Compression Molded and Tape Extruded Samples

To assess the impact of the observed differences in the crystallization process on the prepared samples, the crystallinity X of the propylene in the blend and T_m of the samples prepared by tape extrusion and compression molding were measured. The determination of the X is explained in section 3.6 and the melting enthalpy was equal to the area under the melting peak on DSC curve. The collected data from DSC are presented in Fig. 4.14 and 4.15. Comparison of X and T_m of compression molded samples, as presented in Fig. 4.14, show only minor variations between the samples with different amounts of additives compared to the NP and it was found that the additives at low concentration hardly influenced the crystalline mass fraction and melting point of the polymer. The similar result is observed for most of the samples prepared by the tape extrusion method, as listed in Fig. 4.15. Error measurement is described in section 3.6. Assessment of X of

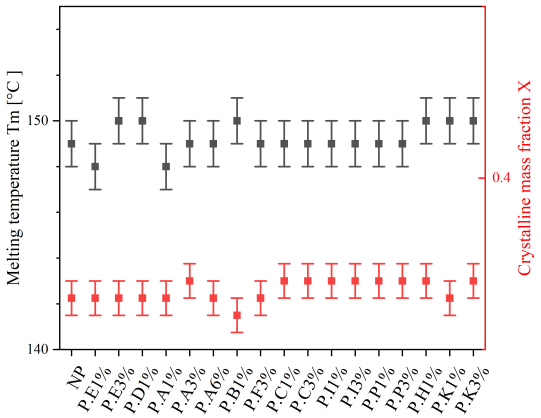

Figure 4.14: Melting temperature T_m and crystalline mass fraction X of NP and melt-blended samples, determined by DSC. Compression molding samples.

the samples prepared by different methods show a slight decrease in the degree of crystallinity of polymer for P.E, P.P, P.H1%, P.A3% and P.K1% in the tape extrusion method. The DSC melting thermograms of the NP and the other blends prepared by compression molding are very similar, and the results for the crystalline mass fraction and the melting temperature did not suggest a change due to additive incorporation. The heat flow curves of NP and P.I1% obtained from the first heating are shown in Fig. 4.16. Comparing the heat flow curves of the first heating for the NP and blends prepared by tape extrusion shows a slight variation in the shape of the peaks. As an example in Fig. 4.17, the second peak prior to the melting peak keeps rising. In P.A6% and P.I this variation is more pronounced and caused a shift in the melting temperature to a lower temperature. It seems that, there is an effect related to the presence of crystals with different stability (different crystallographic forms) or that of lamellae with different thicknesses, possibly followed by a recrystallization process. Schick [44] proposes

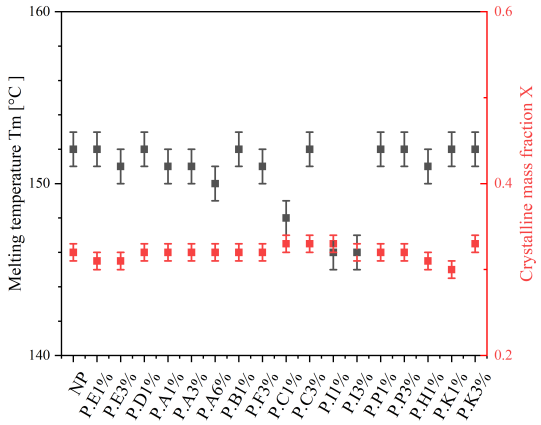

Figure 4.15: Melting temperature T_m and crystalline mass fraction X of NP and melt-blended samples, determined by DSC. Tape extrusion samples.

performing DSC at a higher scanning rate to distinguish between melting and recrystallization phenomena. At higher scanning rates, the recrystallization process is less likely, and the presence of various crystal populations within the sample is possible to distinguish. In general, we can conclude that the changes caused by the addition of liquids only slightly affect how the blends crystallized under the given condition. However, we observe noticeable differences between samples prepared in different ways. A broad melting peak in a DSC thermogram can be an indication of a wide variation in lamellar thickness in polymer or changes in crystallographic form. In the tape extrusion method, there is no control over the cooling rate, and the samples cool down rapidly by exposure to the ambient temperature, which results in a slightly lower degree of crystallinity and a difference in the shape of the melting curves.

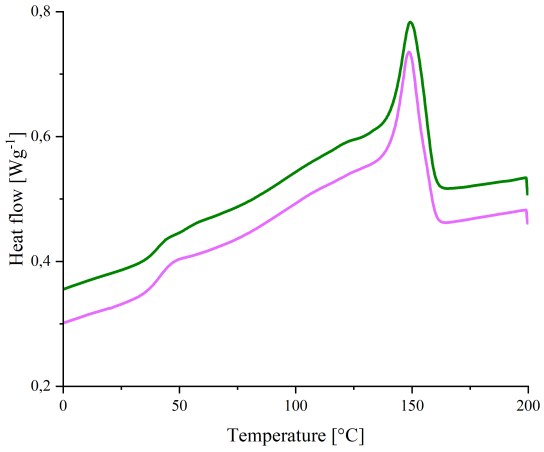

Figure 4.16: Comparison of first heating curve of NP (green curve) with P.I1% (pink curve), determined by DSC. Compression molding samples.

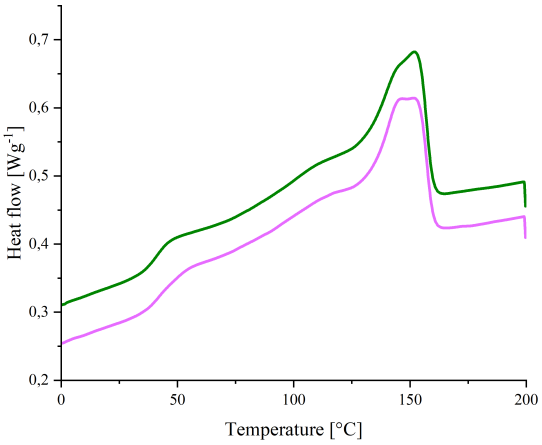

Figure 4.17: Comparison of first heating curve of NP (green curve) with P.I1% (pink curve), determined by DSC. Tape extrusion samples.

4.1.6 Wide Angle X-Ray Scattering

To understand the changes in the samples as a result of different preparation methods, WAXS measurements were performed. Diffraction patterns of the NP and P.A6% prepared by compression molding and tape extrusion are presented in Fig. 4.18.

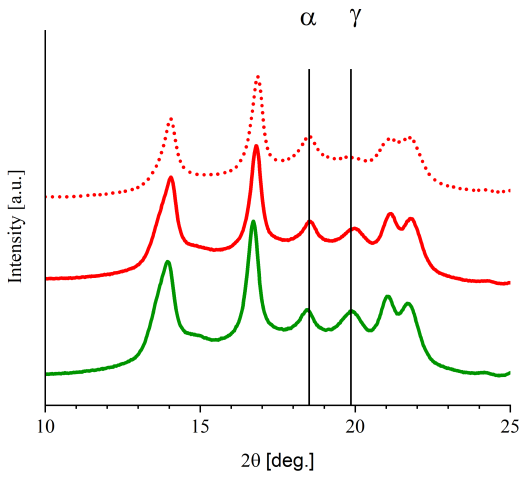

Figure 4.18: Wide angle X-ray scattering diffractogram. NP prepared by CM (green curve), P.A6% prepared by CM (red curve), P.A6% prepared by TE (red dotted curve).

The formation of the α and γ phases in the NP and polymer blends can be identified by their characteristic peaks on the diffractogram. The peaks at angles about 18,5° and 20° indicate the presence of two crystallographic forms of α and γ, respectively. Additionally, P.A6% prepared by compression molding displays a more pronounced

peak for the γ modification, whereas the smaller peak at the same angle for the P.A6%-tape indicates a lower amount of this crystallographic form. As reported by Mezghani et al. [58], γ form is favored during crystallization at higher temperatures, therefore a high cooling rate may suppress the formation of the γ form. We did not observe a big difference in the height of this peak between the NP and P.A6% samples, and only a small decrease in the amount of the γ form is visible for the samples as a result of additive incorporation.

4.1.7 Small Angle X-Ray Scattering

In order to verify the influence of the additive on the crystal structure and to understand where the additive is located, it is necessary to determine the thickness of the amorphous phase and the crystal lamellae by means of SAXS experiment. Changes in the lamellar thickness or aggregation of the additive in the interlamellar distance, can directly influence the properties of blends. The SAXS pattern for NP and that of blends was recorded, and the maximum intensity of the scattering curve for most of the samples, even at low additive concentration, exhibits a shift towards a lower q value. Fig. 4.19 illustrates the scattering profile for P.A6% and P.E3% in comparison with NP. These blends with the highest additive content exhibit the biggest shift towards the lower q value.
The scattering profile for other blends are provided in Fig. 4.20 and 4.21. The

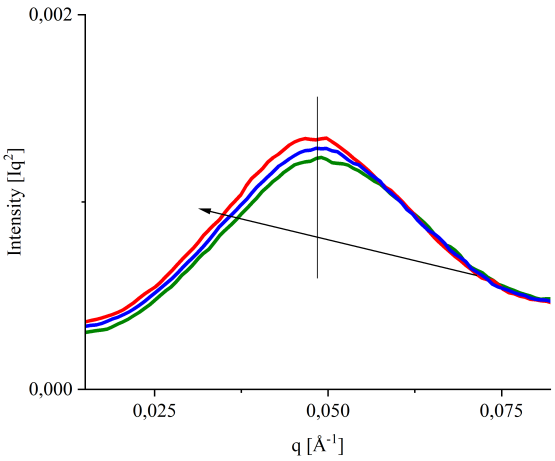

Figure 4.19: Scattering profile of P.A6% and P.E3% in comparison with NP. P.A6% (red), P.E3% (blue) and NP (green).

method used to calculate the long period l_p, X_c, ρ_s, and lamellar thickness l_c were described in section 3.8. Fig. 4.20 presents the results of the long period and their corresponding lamellar thickness. Error of measurement is reported in section 3.8. For X_c, the error of DSC calculated in section 3.6 is reported. A higher change can be observed for the P.E, P.A at higher concentrations, whereas the other blends exhibit the smallest or lack of change. However, even the minor changes within the uncertainty measurement point to an increase in the long period. The relationship between the long period value and the amount of the additive for these two additives is presented in Fig. 4.22. It suggests a similar trend for long period vs. additive concentration. The data from the DSC test do not suggest a change in crystalline mass fraction and melting point, and it can be assumed that the lamellar thickness did not change as a result of additive incorporation. The increase in l_p without significant changes in the l_c suggests that a large part of the additives is in the amorphous phase between the crystalline lamellae. The presence of different crystallographic forms and overlapping of the melting peaks does not allow for an accurate determination of the melting temperature peak.

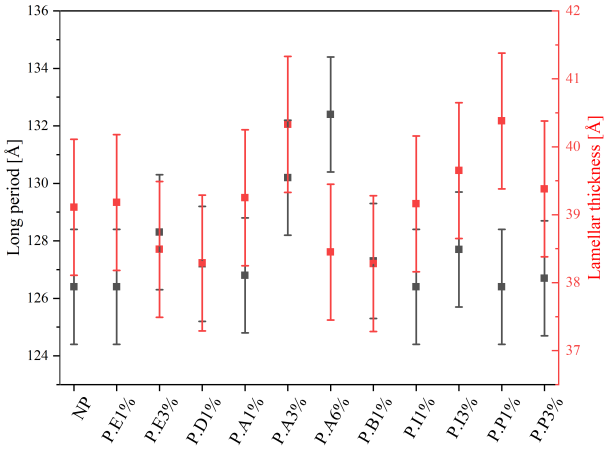

Figure 4.20: Long period and lamellar thickness of the NP and blends, determined by DSC. Compression molding samples.

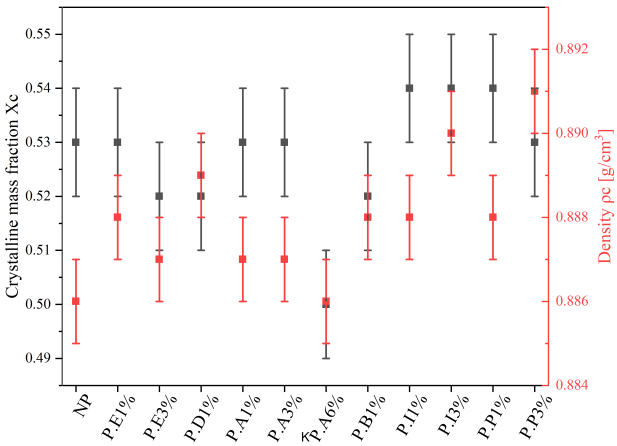

Figure 4.21: Crystalline mass fraction and density of the NP and blends, determined by DSC. Compression molding samples.

The results of the preliminary tests on the materials can be summarized as follows: The thermally stable additives within the temperature range of 200-220°C were determined. LA.G and LA.N were excluded from the additive list due to their low thermal stability in comparable condition. The maximum saturation level of the additives in NP was determined. LA.H and LA.D exhibited the lowest saturation levels of 2,6% and 4%, respectively, while other additives showed saturation levels from 7% to 35%. LA.A showed the highest saturation level. It appeared that the quantification of the additive content in the blend did not yield reliable values for all blends. The study of the kinetics of crystallization suggests a decrease in the rate of crystal growth without significant influence on nucleation process. The degree of crystallinity did not exhibit a significant change as a result of the additive incorporation in polymer blends in both TE and CM preparation methods. A decrease in the amount of γ form was observed for TE samples, which may have resulted from the higher cooling rate in this method. Liquid addititves

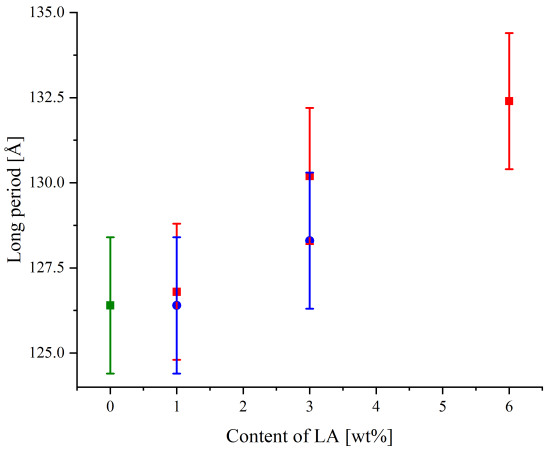

Figure 4.22: Long period variations with additive content. P.A (red), P.E (blue) and NP (green).

only slightly reduced the amount of the γ form. The results from the SAXS test suggest an increase in the interlamellar distance. However,the lamellar thickness and melting temperature did not exhibit a remarkable change. This suggests incorporation of additive in amorphous phase between crystals.

4.2 Material Properties

4.2.1 Thermal Conductivity by Transient Plane Source

The LAs, SAs, and their corresponding thermal conductivity values, which were measured by instrument, are listed in Fig. 4.23. All the additives show a lower thermal conductivity value compared to NP. The values are between 0,211 for SA.K and 0,143 for LA.D. Measurement for SA.I was not possible due to the mechanical properties of the additive (viscous adhesive texture). The determination of measurement error is described in section 3.7. The thermal

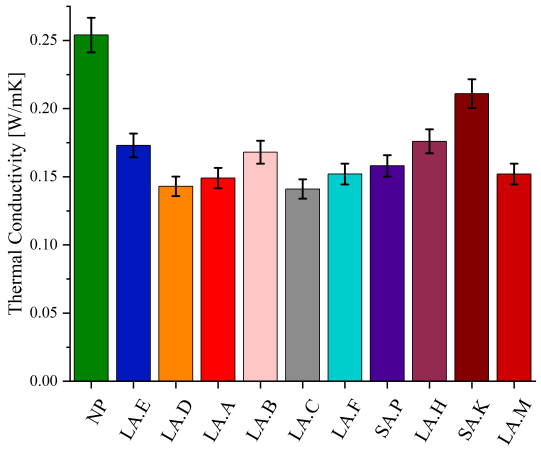

Figure 4.23: Thermal Conductivity of LAs and SAs in comparison with NP tested at 23±0,3°C.

conductivity of the blends was measured, and the obtained values for the NP, and polymer blends are presented in Fig. 4.24. Interestingly, the thermal conductivity of the blends in comparison with that of the NP does not suggest a change. The measured values at various concentrations show only slight variations, that do not exceed the uncertainty of the measurement. It was found that at a very low additive amount ranging from 1% to 3%, the thermal conductivity of the blend remain comparable to that of the base polymer, whereas the thermal conductivity of all additives, according to the results in Fig. 4.23, show lower values compared to NP. It was observed that there was a variety in recorded thermal conductivity between various samples from the same plaque. Interestingly, the observed variations were slightly improved by the sampling from the middle of the plaques. This could be an indication of the existence of a thermal gradient during sample preparation in a hot press machine or inhomogeneity in additive distribution within plaques.

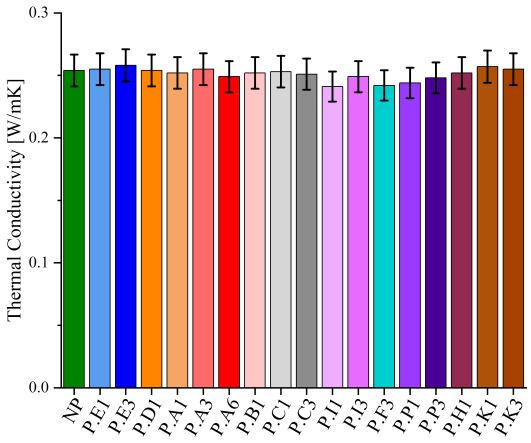

Figure 4.24: Thermal Conductivity of polymer blends in comparison with NP tested at 23±0,3°C.

4.2.2 Dynamic Mechanical Thermal Analysis

For different PP applications, mechanical properties at both low and high temperatures are very important, therefore, DMTA test was carried out. An illustration of the storage modulus, which were recorded at -40°C for different blends, is presented in Fig. 4.25. The determination of the error of measurement is described in section 3.11. The values indicate a decrease in storage modulus upon additive incorporation. The storage modulus of P.A6% with the highest additive content shows a 27% decrease. This result indicates an improvement in the material's stiffness at a very low temperature as a result of additive incorporation, which is a positive effect in the case of this type of material. The values of storage

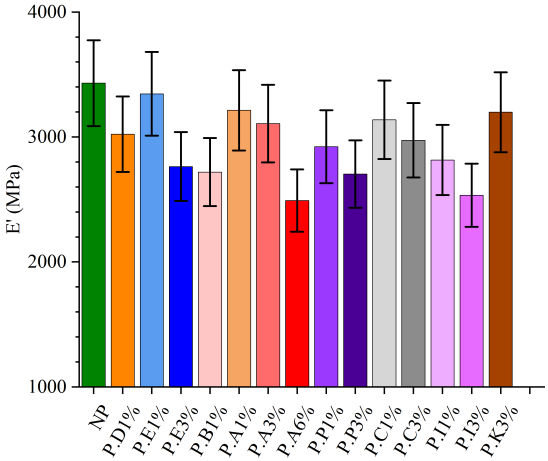

Figure 4.25: DMA storage modulus for polymer blends and NP at -40°C.

modulus at room temperature, 25°C, as presented in Fig. 4.26, suggest a similar declining pattern due to additive inclusion. However, 6% of LA.A strongly reduces the storage modulus to about 50% of the value for NP and only 1% of SA.I affect this value by 34%. Interestingly, polymer blends, including P.A, P.P, and P.C, exhibit a gradual decrease in the storage modulus with increasing additive concentration. Mechanical stability at elevated temperature is a very important parameter in different industrial applications. It was observed that at high temperatures, 130°C, the storage modulus decreased for some of the blends and increased for others. As illustrated in Fig. 4.27, this value may vary from -46% for P.E3% to +32% for P.A1% but still remains at the level of a few MPa. The value of the storage modulus decreases with increasing amount of the LA.A. These observations suggest that the modified polymers can be characterized by a lower modulus compared to the NP. The reduction of storage modulus for blends may be caused by the incorporation of additives in the amorphous phase, which is confirmed by SAXS measurements. In the low strain range that we deal with in DMTA, the properties of the amorphous phase strongly affect the modulus of the samples, which we can see by the reduction of storage modulus. It is important to take into account that various blends showed a declining pattern of modulus in the temperature range of -40 to 130°C to varying extents, and the changes in the

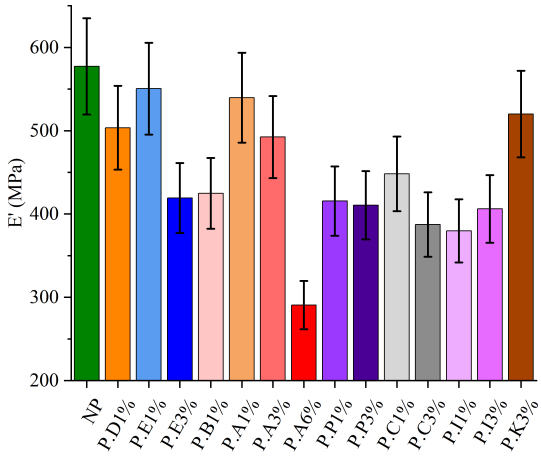

Figure 4.26: DMA storage modulus for polymer blends and NP at 25°C.

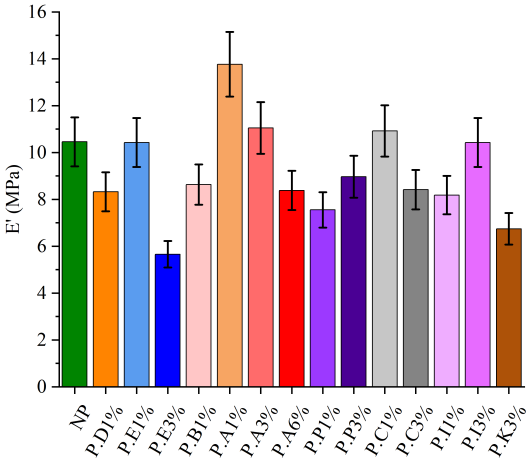

Figure 4.27: DMA storage modulus for polymer blends and NP at 130°C.

storage modulus were not consistent with the additive concentration. To better understand changes in mechanical properties for the blends, measurements of tensile mechanical properties were carried out.

The effect of additives on the glass transition temperature of the polymer matrix and that of the rubber phase is evaluated according to the peaks on loss modulus curves, and the data are presented in Fig. 4.28. As we can see in Fig. 4.29, for both NP and P.A6%, we can observe two separate maxima on the loss modulus plot. One at lower temperature from -50 to -43°C and the other at higher temperature from -12 to -26°C. The first one is related to the glass transition temperature in amorphous EPR, and the second one is to amorphous polypropylene between the lamellae. As can be seen, the T_g of both phases are slightly shifted to a lower temperature. This observation can be attributed to the higher flexibility of the chains in the amorphous phase due to introduction of the additive into the polymer.

It's common knowledge that the chemical structure of the additive and polymer can determine the extent and mechanism of additive-polymer interaction. Fig.

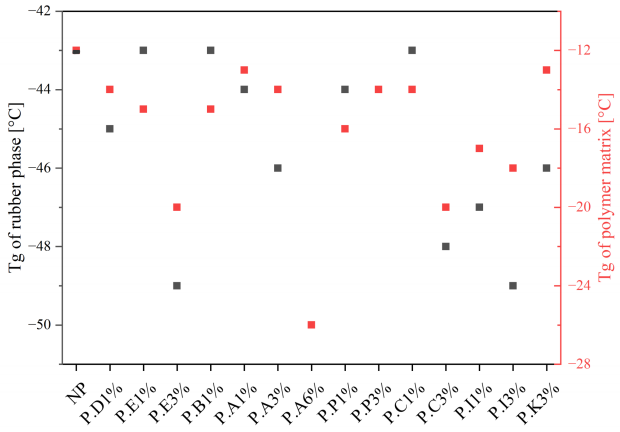

Figure 4.28: Glass transition temperature T_g of the polymer matrix and the rubber phase in NP and other polymer blends.

4.29 presents the reduction in the T_g in P.A6%. As shown, LA.A reduces the glass transition temperature of both polymer phases.
Fig. 4.30 shows the differences between T_g of individual phases for NP and blends. The effectiveness of the additives to influence the T_g of both phases in NP is presented in Fig. 4.30. In most of the samples, the T_g of both phases changed noticeably upon increasing the additive content. Below T_g, modulus is usually higher than above T_g. This change occurs at a lower temperature. One might expect that different additives might be more compatible with EPR or with PP and have different effects on the T_g of these phases. For most of the blends, the variations in glass transition temperatures of both phases were not consistent, and the changes varied with different concentrations. A conclusion regarding the tendency of the liquid toward a specific phase was not possible. Using Scanning Electron Microscopy (SEM) to determine variations in the size of the elastomeric phase (EPR) upon additive incorporation may help estimate the tendency of liquid towards polymer matrix and/or elastomeric phase.

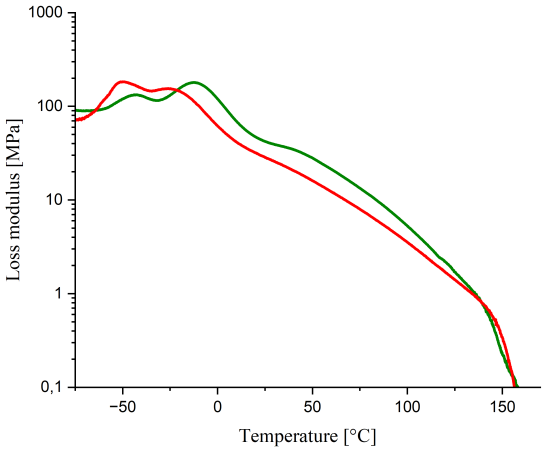

Figure 4.29: Comparison of glass transition temperatures for NP (green) and P.A6% (red).

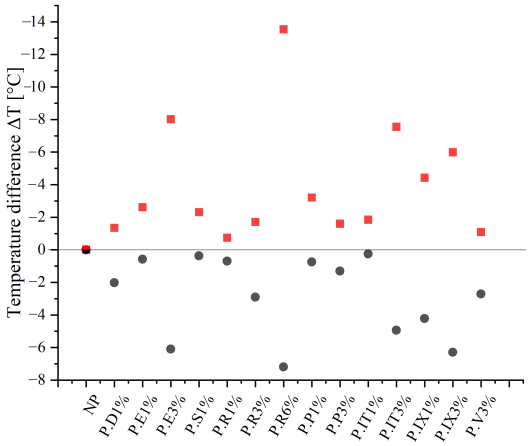

Figure 4.30: Comparison of variations in glass transition temperature of matrix and rubber phase. Rubber phase in black color and matrix in red color.

4.2.3 Mechanical Testing

To evaluate the impact of additives on the mechanical response of the polymer, the specimens were subjected to a constant strain, and the mechanical response of the material was recorded. The stress-strain curve has been presented in Fig. 4.31. All blends show a mechanical behavior similar to that of the NP. At very low strain, reversible deformation occurs in the amorphous phase. As the strain increases, plastic deformation and irreversible changes in the lamellae, including the lamellae rotation followed by its deformation, occur. The resistance of lamellae to deformation is reflected by an increase in the stress (yield point). By increasing applied strain, the changes in the cross-section of the sample (necking) cause a drop in the force until the curve reaches a very short plateau which indicates reorientation of the lamellae. In this step the deformation is not constant. Further increase in the strain causes an increase in the stiffness of the sample without changing its cross-section. This is due to alignment of the crystals in the drawing direction, and it is accompanied with the stretch of the amorphous phase. It is noteworthy to mention that the color change in the sample is attributed to the void formation at the interface of the crystal and amorphous phase. This leads to light scattering, which is known as the stress whitening mechanism. At a very high strain, the sample fractures. It was observed that the additives did not significantly change the general mechanical behavior of the NP. The results of the tensile test are summarized in

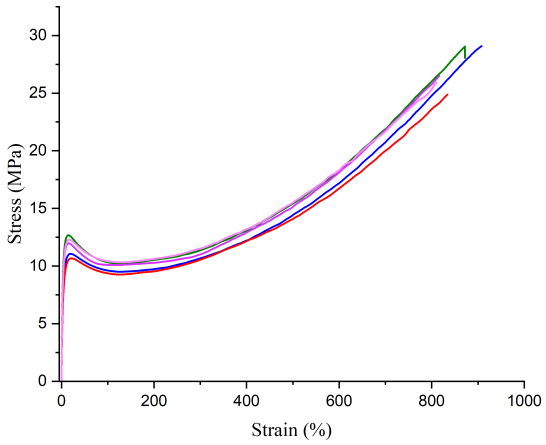

Figure 4.31: Stress-Strain curve recorded during tensile deformation. NP (green curve), P.I3% (pink curve), P.P3% (violet curve), P.E3% (blue curve), P.A6% (red curve).

Fig. 4.32 and 4.33, which contain values for the tensile modulus E, yield stress σ, stress at break σ and elongation at break ϵ recorded from the tensile test for NP and all blends. The determination of measurement error is described in section 3.10. For all samples, we can observe that the tensile modulus of the samples decreases with the increase in the content of additives, although the values depend on the type of additive. At a very low concentration, the value of tensile modulus exhibits a slight decrease in all the samples. For samples with an additive content of 1%, the

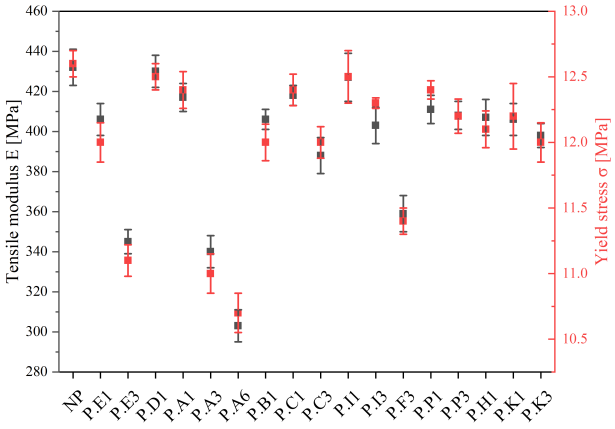

Figure 4.32: Mechanical properties of different tape extruded polymer blends

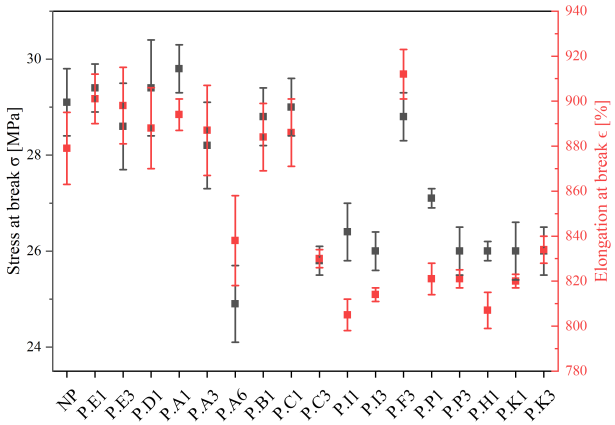

Figure 4.33: Mechanical properties of different tape extruded polymer blends

greatest changes are observed for materials including P.E, P.B, P.H, P.K, with a 6% reduction, and for materials including P.D and P.I, this difference is minimal. For 3% additives, P.P exhibits the smallest changes of 5% while this value decreases to up to 17% for P.I3, P.K, P.C, P.A, P.F. For LA.A and LA.E, we observed a decrease of approximately 20%. The lowest value was noted for P.A6%, where the modulus decreases by 30%. These results are presented in Fig. 4.32. The values for yield stress follow a similar decrease trend. Similar to the tensile modulus, the lowest values are for P.A samples, although the changes are at the level of 15% for P.A6%. As presented in Fig. 4.33, stress at break is slightly affected and displays a lower value as a result of the highest concentration of the additives in P.C, P.I, P.P and P.K polymer blends. However, considering the error bar, the changes are less than 6%. Stress at break was less affected by LA.A and LA.E at lower concentrations, but 6% of the LA.A reduced this property by 14%. Interestingly, 3% of P.C, P.I, P.P and P.K reduce this property by approximately 11%, while even the lowest amount of SA.P and SA.I shows similar results. Amongst them, 1% of LA.H affects this property similarly. The value of the elongation at break does not suggest a

significant change for most of the blends and varies between +4% to -8% without clearly suggesting a trend for content or type of the additive.
As presented in Fig. 4.34, P.A6% exhibits the lowest tensile modulus and yield stress with the highest additive content. It shows the lowest resistance to the applied strain and reflect the softness of the material caused by the additive introduced to the polymer.

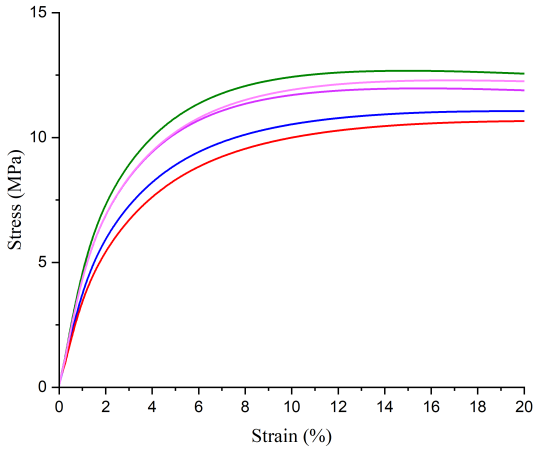

Figure 4.34: Stress-Strain curve recorded during tensile deformation. NP (green curve), P.I3% (pink curve), P.P3% (violet curve), P.E3% (blue curve), P.A6% (red curve).

As shown in Fig. 4.35, there is a clear relationship between the decreasing value of the tensile modulus and the increasing content of the additive. Fig. 4.36 clearly illustrates the dependency of the yield stress on the additive content. It continuously decreases upon additive incorporation.

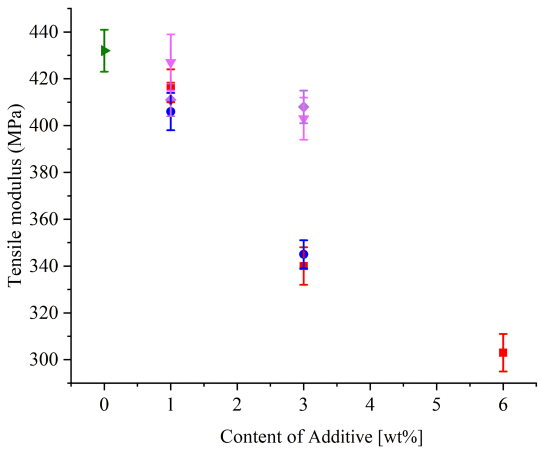

Figure 4.35: Comparison of tensile modulus with varying content for LA.E (blue), LA.A (red), SA.I (pink) and SA.P (violet) in blend with NP(green).

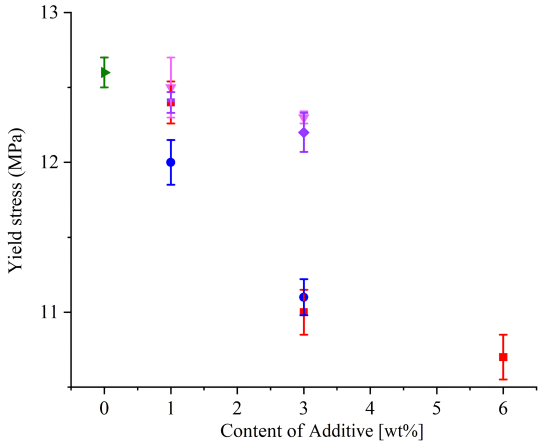

Figure 4.36: Comparison of yield stress with varying content for LA.E (blue), LA.A (red), SA.I (pink) and SA.P (violet) in blend with NP (green).

DSC results have shown quite similar degrees of crystallinity for all samples, and in the SAXS experiment, we observed an increase in the interlamellar distance in the polymer blends, which was potentially caused by additive aggregation in this area. It was found that the lamellar thickness remained nearly constant with increasing additive concentration.
Fig. 4.37 presents the yield stress of the polymer blends with the corresponding long period measured by SAXS. In general, we observe a decrease in the Young's modulus with no decrease in the elongation at break, which, in the case of PP-based materials has a very positive effect. Tensile modulus is closely related to

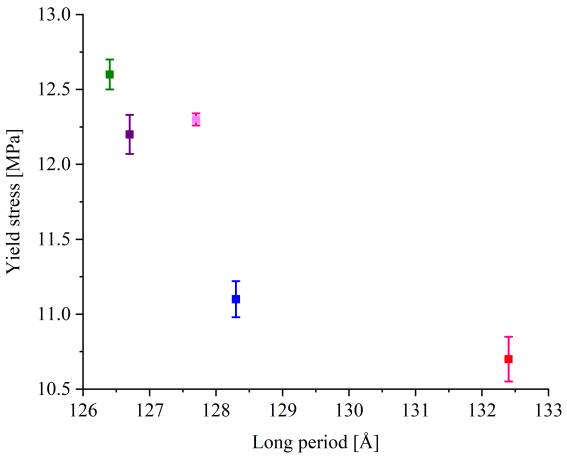

Figure 4.37: Yield stress vs. long period. NP (green), P.P3% (violet), P.I3% (pink), P.E3% (blue), and P.A6% (red).

the deformation of the amorphous phase in the polymer, which is why its changes with the liquid content are so strong. The observed decrease in yield stress can be

attributed to the phenomenon explained as follows: during crystallization, additives are expelled from the crystal, and these are probably localized in the interlamellar region. Introducing the additive into the polymer leads to swelling in the amorphous region, which causes an increase in the interlamellar distance. The chains connecting crystals will be stretched, and crystals will be under tension. It creates a negative stress within the lamellae and leads to its pre-tension. Consequently, less energy is required to activate the plastic deformation mechanism [59][60].

5

Conclusion

The results of the saturation test indicated the maximum amount of the liquid incorporation without phase separation.
In the exudation test, it was observed that polymer blends containing 3% additive, did not exhibit a remarkable migration of the additive to the surface.
A high cooling rate in tape extrusion sample preparation method may resulted in the formation of a lower amount of the γ-phase; However, the presence of the additive in blends did not exhibit a significant change in the degree of crystallinity.
Most of the additives were thermally stable at processing temperature and did not strongly affect the thermal stability of the blends.
The rate of crystallization was slowed upon additive incorporation. However, it did not strongly affect crystallinity, and lamellar thickness.
The incorporation of additives with a lower thermal conductivity than the polymer, did not significantly affect the thermal conductivity of the polymer blends.
Additives have shown a plasticizing effect on the polymer blend, by reducing the modulus of the material at low and medium temperatures, suggesting an improvement of the mechanical properties without deterioration of the thermal stability at high temperature. Furthermore, they caused a decrease in the glass transition temperature of both amorphous and elastomeric phase, which indicates the additive tendency towards both phases. Additives may partially accumulate in the interlamellar distance, which can lead to an increase in the interlamellar distance without having an influence on the crystal thickness. The variation in lamellar thickness was confirmed by SAXS results. The presence of liquid in the amorphous phase of the matrix strongly decreases the modulus of the samples. An increase in the interlamellar distance due to additive incorporation exhibited an influence on plastic deformation mechanism, resulting in a decrease in yield stress. The additives led to swelling of the amorphous phase, which might change the stress distribution in the system and resulted in a decrease in the required energy for deformation of the crystals.

Bibliography

[1] Valentina Marturano, Pierfrancesco Cerruti, and Veronica Ambrogi. Polymer additives. *Physical Sciences Reviews*, 2(6):139–170, 2017.

[2] Ernest A Coleman. Plastics additives. In *Applied Plastics Engineering Handbook*, pages 489–500. Elsevier, 2017.

[3] Hisham Maddah. Polypropylene as a promising plastic: A review. *American Journal of Polymer Science*, 6(1):1–11, 2016.

[4] C. E. H. Bawn and A. Ledwith. Stereoregular addition polymerisation. *Q. Rev. Chem. Soc.*, 16(4):361–434, 1962.

[5] L. Lin and A. Argon. Review structure and plastic deformation of polyethylene. *Journal of Materials Science*, 29(2):294–323, 1994.

[6] J. N. Tomlinson, D. E. Kline, and J. A. Sauer. Effect of nuclear radiation on the thermal conductivity of polyethylene. *Polymer Engineering & Science*, 5(1):44–48, 1965.

[7] Cornelia Kock, Markus Gahleitner, Alois Schausberger, and Elisabeth Ingolic. Polypropylene/polyethylene blends as models for high-impact propyleneethylene copolymers, part 1: Interaction between rheology and morphology. *Journal of Applied Polymer Science*, 128(3):1484–1496, 2013.

[8] Markus Gahleitner, Cornelia Tranninger, and Petar Doshev. Heterophasic copolymers of polypropylene: Development, design principles, and future challenges. *Journal of Applied Polymer Science*, 130(5):3028–3037, 2013.

[9] Michiel F. Bergstra, Peter Denifl, Markus Gahleitner, Dusan Jeremic, Vasileios Kanellopoulos, Daniela Mileva, Pavel Shutov, Vasileios Touloupidis, and Cornelia Tranninger. Polymerization in the borstar polypropylene hybrid process: Combining technology and catalyst for optimized product performance. *Polymers*, 14(21):4763, 2022.

[10] Giuliano Cecchin, Giampiero Morini, and Anteo Pelliconi. Polypropene product innovation by reactor granule technology. *Macromolecular Symposia*, 173(1):195–210, 2001.

[11] Carsten Dingler, Klaus Dirnberger, and Sabine Ludwigs. Semiconducting polymer spherulitesfrom fundamentals to polymer electronics. *Macromolecular Rapid Communications*, 40(1):1800601, 2019.

[12] B Monasse and JM Haudin. Growth transition and morphology change in polypropylene. *Colloid and Polymer Science*, 263:822–831, 1985.

[13] Kohji Tashiro. *Handbook of Polymer Crystallization*, chapter 5, pages 165–196. John Wiley & Sons, Ltd, 2013.

[14] B. Lotz and J. C. Wittmann. The molecular origin of lamellar branching in the (monoclinic) form of isotactic polypropylene. *Journal of Polymer Science Part B: Polymer Physics*, 24(7):1541–1558, 1986.

[15] Andrew J. Lovinger, Jaime O. Chua, and Carl C. Gryte. Studies on the alpha and beta forms of isotactic polypropylene by crystallization in a temperature gradient. *Journal of Polymer Science: Polymer Physics Edition*, 15(4):641–656, 1977.

[16] Stefano Meille and Sergio Brückner. Non-parallel chains in crystalline gamma-isotactic polypropylene. *Nature*, 340:455–457, 08 1989.

[17] A Turner-Jones. Development of the gamma-crystal form in random copolymers of propylene and their analysis by dsc and x-ray methods. *Polymer*, 12(8):487–508, 1971.

[18] E. Lezak, Z. Bartczak, and A. Galeski. Plastic deformation of the gamma phase in isotactic polypropylene in plane-strain compression. *Macromolecules*, 39(14):4811–4819, 2006.

[19] Ph Tordjeman, C Robert, G Marin, and P Gerard. The effect of α, β crystalline structure on the mechanical properties of polypropylene. *The European Physical Journal E*, 4:459–465, 2001.

[20] Darrell R. Morrow and. Polymorphism in isotactic polypropylene. *Journal of Macromolecular Science, Part B*, 3(1):53–65, 1969.

[21] Sune Pettersson and G.D. Mahan. Theory of the thermal boundary resistance between dissimilar lattices. *Physical Review B*, 42(12):7386 7390, 1990.

[22] D. Hansen and G. A. Bernier. Thermal conductivity of polyethylene: The effects of crystal size, density and orientation on the thermal conductivity. *Polymer Engineering & Science*, 12(3):204–208, 1972.

[23] Wen bin Zhang, Zhi xing Zhang, Jing hui Yang, Ting Huang, Nan Zhang, Xiao tong Zheng, Yong Wang, and Zuo wan Zhou. Largely enhanced thermal conductivity of poly(vinylidene fluoride)/carbon nanotube composites achieved by adding graphene oxide. *Carbon*, 90:242–254, 2015.

[24] A.S. Luyt, J.A. Molefi, and H. Krump. Thermal, mechanical and electrical properties of copper powder filled low-density and linear low-density polyethylene composites. *Polymer Degradation and Stability*, 91(7):1629–1636, 2006.

[25] Yanfei Xu, Daniel Kraemer, Bai Song, Zhang Jiang, Jiawei Zhou, James Loomis, Jianjian Wang, Mingda Li, Hadi Ghasemi, Xiaopeng Huang, Xiaobo Li, and Gang Chen. Nanostructured polymer films with metal-like thermal conductivity. *Nature Communications*, 10(1), 2019.

[26] Hong He, Renli Fu, Yuan Shen, Yanchun Han, and Xiufeng Song. Preparation and properties of si3n4/ps composites used for electronic packaging. *Composites Science and Technology*, 67(11):2493–2499, 2007.

[27] Karnthidaporn Wattanakul, Hathaikarn Manuspiya, and Nantaya Yanumet. The adsorption of cationic surfactants on bn surface: Its effects on the thermal conductivity and mechanical properties of bn-epoxy composite. *Colloids and Surfaces A: Physicochemical and Engineering Aspects*, 369(1):203–210, 2010.

[28] Yu Jia, Han Zhang, and Jun Zhang. The effect of peroxide cross-linking on the thermal conductivity and crystallinity of low-density polyethylene. *Materials Today Communications*, 31:103735, 2022.

[29] Koh-Hei Nitta and Motowo Takayanagi. Role of tie molecules in the yielding deformation of isotactic polypropylene. *Journal of Polymer Science Part B: Polymer Physics*, 37(4):357–368, 1999.

[30] PB Bowden and RJ Young. Deformation mechanisms in crystalline polymers. *Journal of Materials Science*, 9:2034–2051, 1974.

[31] Qamer Zia, Hans-Joachim Radusch, and René Androsch. Deformation behavior of isotactic polypropylene crystallized via a mesophase. *Polymer Bulletin*, 63:755–771, 11 2009.

[32] Anton Peterlin. Molecular model of drawing polyethylene and polypropylene. *Journal of Materials Science*, 6:490–508, 1971.

[33] Wenbing Hu, Vincent B. F. Mathot, Rufina G. Alamo, Huanhuan Gao, and Xuejian Chen. *Crystallization of Statistical Copolymers*, chapter 1, pages 1–43. Springer International Publishing, Cham, 2017.

[34] Bernhard Wunderlich. *Thermal Analysis of Polymeric Materials*, chapter 4, pages 279–454. Springer Berlin Heidelberg, 2005.

[35] Abi Munajad, Cahyo Subroto, and Suwarno. Fourier transform infrared (ftir) spectroscopy analysis of transformer paper in mineral oil-paper composite insulation under accelerated thermal aging. *Energies*, 11(2):364, 2018.

[36] Andreas Gupper and Sergei G. Kazarian. Study of solvent diffusion and solvent-induced crystallization in syndiotactic polystyrene using ft-ir spectroscopy and imaging. *Macromolecules*, 38(6):2327–2332, 2005.

[37] L Barbeş, C Rădulescu, and C Stihi. Atr-ftir spectrometry characterisation of polymeric materials. *Romanian Reports in Physics*, 66(3):765–777, 2014.

[38] Ling Zhao, Shi-Ling Jia, Ze-Peng Wang, Yun-Jing Chen, Jun-Jia Bian, Li-Jing Han, Hui-Liang Zhang, and Li-Song Dong. Thermal, rheological and mechanical properties of biodegradable poly (propylene carbonate)/epoxidized soybean oil blends. *Chinese Journal of Polymer Science*, 39:1572–1580, 2021.

[39] Yu Lin, Langping Liu, Gangmin Xu, Dongge Zhang, Aiguo Guan, and Guozhang Wu. Interfacial interactions and segmental dynamics of poly(vinyl acetate)/silica nanocomposites. *The Journal of Physical Chemistry C*, 119(23):12956–12966, 2015.

[40] Thomas G. Mayerhöfer, Susanne Pahlow, and Jürgen Popp. The bouguer-beer-lambert law: Shining light on the obscure. *ChemPhysChem*, 21(18):2029–2046, 2020.

[41] Artur Rozanski, Marta Safandowska, and Artur Krajenta. Dsc/saxs analysis of the thickness of lamellae of semicrystalline polymers-restrictions in the case of materials with swollen amorphous phase. *Polymer Testing*, 65:189–196, 2018.

[42] Joanna Drzeżdżon, Dagmara Jacewicz, Alicja Sielicka, and Lech Chmurzyński. Characterization of polymers based on differential scanning calorimetry based techniques. *TrAC Trends in Analytical Chemistry*, 110:51–56, 2019.

[43] M. Mucha and Z. Królikowski. Application of dsc to study crystallization kinetics of polypropylene containing fillers. *Journal of Thermal Analysis and Calorimetry*, 74(2):549 557, 2003.

[44] Christoph Schick. Differential scanning calorimetry (dsc) of semicrystalline polymers. *Analytical and bioanalytical chemistry*, 395:1589–611, 2009.

[45] Yi He. Rapid thermal conductivity measurement with a hot disk sensor: Part 1. theoretical considerations. *Thermochimica Acta*, 436(1):122–129, 2005.

[46] Ronald J. Warzoha and Amy S. Fleischer. Determining the thermal conductivity of liquids using the transient hot disk method. part i: Establishing transient thermal-fluid constraints. *International Journal of Heat and Mass Transfer*, 71:779–789, 2014.

[47] Silas E Gustafsson, Besira M Mihiretie, and Mattias K Gustavsson. Measurement of thermal transport in solids with the hot disc method. *International Journal of Thermophysics*, 45(1):1, 2024.

[48] Benjamin Chu and Benjamin S. Hsiao. Small-angle x-ray scattering of polymers. *Chemical Reviews*, 101(6):1727–1762, 2001.

[49] J.M.G. Cowie and V. Arrighi. *Polymers:Chemistry and Physics of Modern Materials, Third Edition(3re ed.)*, chapter 10, pages 253–277. CRC Press, 2007.

[50] Hsin-Lung Chen, Lain-Jong Li, and Tsang-Lang Lin. Formation of segregation morphology in crystalline/amorphous polymer blends: molecular weight effect. *Macromolecules*, 31(7):2255–2264, 1998.

[51] Witold Brostow. *Mechanical Properties*, chapter 24, pages 423–445. Springer New York, 2007.

[52] J.M.G. Cowie and V. Arrighi. *Polymers:Chemistry and Physics of Modern Materials, Third Edition(3re ed.)*, chapter 13, pages 345–388. CRC Press, 2007.

[53] Kevin P. Menard and Noah R. Menard. *Dynamic Mechanical Analysis in the Analysis of Polymers and Rubbers*, chapter 1-2, pages 1–33. John Wiley & Sons, Ltd, 2015.

[54] Muhammad Ahsan Bashir. Use of dynamic mechanical analysis (dma) for characterizing interfacial interactions in filled polymers. *Solids*, 2(1):108–120, 2021.

[55] Isaac O. Igwe, Chinomso M. Ewulonu, and Ifeoma Igboanugo. Studies on the diffusion characteristics of some aromatic solvents into polypropylene film. *Journal of Applied Polymer Science*, 102(2):1985–1989, 2006.

[56] T. Nishi and T. T. Wang. Melting point depression and kinetic effects of cooling on crystallization in pvf2-pmma mixtures. *Macromolecules*, 8(6):909–915, 1975.

[57] Stanislaw Galeski, Ewa Piorkowska, Artur Rozanski, Gilles Regnier, Andrzej Galeski, and Kinga Jurczuk. Crystallization kinetics of polymer fibrous nanocomposites. *European Polymer Journal*, 83:181–201, 2016.

[58] Khaled Mezghani and Paul J. Phillips. Gamma-phase in propylene copolymers at atmospheric pressure. *Polymer*, 36(12):2407–2411, 1995.

[59] Artur Krajenta and Artur Rozanski. Physical state of the amorphous phase of polypropylene-influence on thermo-mechanical properties. *Polymer*, 70:127–138, 2015.

[60] Artur Rozanski. Miscible/partially-miscible blends of polypropylenethe mechanisms responsible for the decrease of yield stress. *Journal of Polymer Science Part B: Polymer Physics*, 56(17):1203–1214, 2018.

DEPARTMENT OF SOME SUBJECT OR TECHNOLOGY
CHALMERS UNIVERSITY OF TECHNOLOGY
Gothenburg, Sweden
www.chalmers.se

CHALMERS
UNIVERSITY OF TECHNOLOGY